Dynamic interactions between groundwater level and discharge by phreatophytes

Cheng-Wei Huang[1,2], Jean-Christophe Domec[3,4], Thomas L O'Halloran[5,6], and Samantha Hartzell[1]

[1]Department of Civil and Environmental Engineering, Portland State University, Portland, Oregon 97201, USA
[2]Oregon Water Resources Department, Salem, Oregon 97301, USA
[3]Bordeaux Sciences Agro, UMR 1391 INRAE-ISPA, 33170, Gradignan, France
[4]Nicholas School of the Environment, Duke University, Durham, North Carolina 27708, USA
[5]Belle W. Baruch Institute of Coastal Ecology and Forest Science, Clemson University, Georgetown, South Carolina 29440, United States
[6]Forestry and Environmental Conservation Department, Clemson University, Clemson, South Carolina 29634, USA

June 26, 2025

Abstract

Many traditional models that predict plant groundwater use based on groundwater level variations, such as the White method, make various simplifying assumptions. For example, these models often neglect the role of plant hydraulic redistribution, a process that can contribute up to 80% of transpiration. Thus, this work aims to avoid such assumptions and subsequently explore the dynamic interactions between groundwater levels and phreatophytic vegetation, including plant nocturnal transpiration, hydraulic redistribution, and response to atmospheric conditions, in shallow-groundwater ecosystems using Loblolly pine (*Pinus taeda*) as a model species. The model scenarios are formulated using a stomatal-optimization model coupled to the soil-plant-atmosphere continuum. Flow through soil and groundwater are described using the Richards equation and a linear reservoir approximation, respectively, with groundwater in contact with an external water body of fixed elevation. Results show that nocturnal transpiration, mediated by plant residual conductance, and hydraulic redistribution, are able to reduce groundwater levels at night and alter the groundwater recharge rate. Projected atmospheric conditions of increased carbon dioxide and elevated temperature have opposing effects on groundwater levels, which tend to roughly cancel each other under a projected scenario of 500 ppm carbon dioxide and 1.5 C warming. Such detailed modeling can be used to provide further insights into coupled interactions between vegetation, climate and groundwater levels in phreatophyte-dominated ecosystems.

groundwater, hydraulic redistribution, nocturnal transpiration, phreatophytes, root water uptake, Loblolly pine (*Pinus taeda* L)

1 Introduction

Groundwater has been used as the main source of drinking water for more than two billion people at the global scale (Morris et al., 2003; UNESCO World Water Assessment Programme

(WWAP), 2022). Globally, 42% of irrigation water, 36% of household water, and 27% of manufacturing water withdrawals are from groundwater (Döll et al., 2012; Gleeson et al., 2020). In the US High Plains, groundwater resources supported up to 90% of irrigation and produced 3 billion US dollars from 1960–2007 (García Suárez et al., 2019). However, in many semi-arid and arid areas (including central and southern US High Plains) groundwater withdrawals have far exceeded aquifer recharge rates in recent years (McGuire, 2017; Scanlon et al., 2010; Siebert et al., 2010). When such significant imbalances between withdrawals and recharge persists, the groundwater in these areas can be viewed as a nonrenewable resource (Ahmed and Umar, 2009; Scanlon et al., 2007). Much work has gone into assessing groundwater storage and understanding the sustainability of groundwater systems in the face of human-caused depletion (Rateb et al., 2020; Scanlon et al., 2023; Siebert et al., 2010).

In order to adequately evaluate the sustainability of groundwater withdrawals, natural groundwater discharge mechanisms and volumes must also be considered. Water loss through plants (i.e., transpiration) often cannot be overlooked, especially when groundwater tables are shallow and/or rooting systems are particularly deep. Phreatophytes uptake most of their water requirements from the saturated zone (Cooper et al., 2006; Laczniak et al., 1999; Naumburg et al., 2005). For example, groundwater discharge though phreatophytes in Dixie Valley and Margosa Desert, Nevada can be up to 61% and 37% of total evapotranspiration, respectively (Garcia et al., 2015; Moreo et al., 2017). When compared to bare soil conditions, a 50 cm drop in mean groundwater level was predicted by a modeling study with a description of stochastic precipitation process for recharge in loamy sand soil with deep rooted vegetation (Laio et al., 2009). In such groundwater-dependent ecosystems, groundwater depth further dictates ecosystem structure (i.e., plant community composition and distribution) and functioning (Eamus et al., 2006), and the presence of groundwater may increase ecosystem resilience to prolonged droughts (Koirala et al., 2017; Orellana et al., 2012). It is for these reasons that accurate estimation of the dynamic relation between groundwater level and withdrawal by phreatophytes continues to draw significant research attention in hydrological, ecological, and biogeochemical sciences (Hernandez, 2022; Rodriguez-Iturbe et al., 2007).

Thus, this study aims to develop a modeling framework that more accurately represents the dynamic relationship between groundwater levels and plant water withdrawals. Understanding such dynamic interactions is a vexing problem because fluctuations in groundwater levels can be further impacted by various recharge and discharge processes (Jiang et al., 2017). Previous modeling studies have made various assumptions around these dynamics, which are reviewed here to illustrate how a more refined modeling approach might provide further information about the interrelated interactions between vegetation and the water table.

In recent decades, the White method (WM) (White, 1932) and its variants—such as the water table fluctuation method (Carlson Mazur et al., 2014a; Fahle and Dietrich, 2014; Gribovszki, 2018; Orellana et al., 2012; Soylu et al., 2012; Wang et al., 2014; Yin et al., 2013; Zhu et al., 2011)—have utilized groundwater level fluctuations (i.e., hydrographs) to estimate groundwater consumption by plants (i.e., transpiration) across various timescales. However, the WM makes several assumptions about the interaction between vegetation and the water table. The WM first assumes that the diurnal pattern of transpiration is the primary process shaping the diurnal fluctuation of groundwater levels. However, various factors—such as changes in precipitation input, cyclic pumping rates, barometric pressure, alternating freeze/thaw events, Lisse effects, and connections to external water bodies—can also influence diurnal groundwater-level fluctuations (Domec et al., 2012b; Healy and Cook, 2002; Todd and Mays, 2004). Another assumption embedded in the WM is that of a constant daily recharge or discharge rate. This assumption is often invalid, even when lateral flow between the targeted groundwater body and an external water body is the only source of recharge or discharge, aside from water withdrawals by

phreatophytes (such as during dry periods with little to no rainfall). Specifically, the rate of lateral recharge can vary with diurnal fluctuations in groundwater levels, even when the water level of the external water body remains constant (Laio et al., 2009; Ridolfi et al., 2008). Therefore, the proposed modeling approach in this study accounts for the connection between groundwater and external water bodies and explores how the non-constant recharge rate induced by external water bodies impacts groundwater dynamics.

Another assumption adopted by the WM is that nocturnal groundwater withdrawal through plants can be neglected. However, several experiments (Caird et al., 2007; Dawson et al., 2007; Huang et al., 2015; Novick et al., 2009) have shown that nocturnal transpiration can account for 10-30% of daily transpiration. Additionally, hydraulic redistribution—the movement of water from wet to dry soil layers through the root system—commonly occurs at night and can contribute up to 80% of daily transpiration, as demonstrated by several experimental and modeling studies (Domec et al., 2010; Neumann and Cardon, 2012). Moreover, it is not uncommon for plants to refill their internal water storage at night by drawing water directly from both the saturated and unsaturated zones (see review in Huang et al. (2017)). These findings suggest that nocturnal plant activity can significantly impact groundwater dynamics, especially when rooting depth is sufficient to reach groundwater (Domec et al., 2012a). Consequently, the proposed modeling framework accounts for the widely observed phenomena of nocturnal transpiration and hydraulic redistribution, and their roles in groundwater dynamics are examined.

Finally, the WM uses a single value of specific yield to represent the overall water release from the saturated soil column as groundwater levels fluctuate. However, specific yield can vary with groundwater levels and different soil water statuses in the unsaturated zone (Bear, 1988; Fahle and Dietrich, 2014; Gribovszki, 2018; Healy and Cook, 2002; Loheide et al., 2005; Nachabe, 2002). This variability suggests that factors such as capillary rise, hydraulic redistribution through plant rooting systems (Domec et al., 2012a; Mooney et al., 1980; Neumann and Cardon, 2012), and nocturnal replenishment of plant water storage can also impact specific yield, thereby influencing the estimation of water consumption by phreatophytes when using the WM. Therefore, the proposed modeling approach incorporates soil water dynamics that allow for variations in specific yield over time, particularly when accounting for hydraulic redistribution.

A recent review covering many previous modeling and experimental studies (Wang et al., 2023) indicated that the lack of a more realistic representation of rhizosphere processes remains a significant barrier for process-based modeling frameworks in providing more accurate estimates of plants' groundwater consumption. Many different approaches have been taken over time to elucidate the dynamics and drivers of plant-groundwater interactions. For instance, the energy balance method (Nichols, 1993, 1994) has been used to estimate the soil evaporation and plant transpiration. When adopting such a method, a relation between groundwater level and plant transpiration can be subsequently developed to estimate groundwater consumption by plants (Domec et al., 2012b). However, this method does not account for the partitioning of root water uptake between the saturated and unsaturated zones.

Other studies have explored rhizosphere processes in more detail. For example, Loheide et al. (2005), have explored how groundwater levels are impacted by various aquifer geometries and soil properties, using a saturated-unsaturated flow model (VS2D) (Hsieh et al., 2000) with a pre-set constant and uniformly distributed root water uptake. Similarly, Grimaldi et al. (2015) used HYDRUS 2D (Simunek and Van Genuchten, 1999) to explore how different soil types and root distributions impact the dynamics of groundwater level, given a pre-set constant potential root water uptake adjusted by a water stress function (Feddes et al., 1976). Laio et al. (2009) further considered stochastic precipitation (as a marked Poisson process) as an additional recharge source in the modeling system, while Zhu et al. (2019) and Zhang et al. (2022) used the SiTH (Simple Terrestrial Hydrosphere) model to explore the contribution of different water

paths (e.g., soil evaporation and transpiration from saturated and unsaturated zone) to the total evapotranspiration. However, none of these modeling frameworks accounted for the effects of hydraulic redistribution and nocturnal transpiration. The pre-specified root water uptake or potential evapotranspiration in these studies also suggests that such approaches fail to capture how groundwater level is impacted by the dynamic partitioning of root water uptake between saturated and unsaturated zones.

In another study, Gou and Miller (2014) accounted for the effects of hydraulic redistribution on plant groundwater usage through the development of a groundwater–soil–plant–atmosphere continuum model, which was later incorporated into a distributed groundwater-land surface model (Gou et al., 2018), ParFlow-CLM (Kollet and Maxwell, 2006, 2008; Maxwell and Miller, 2005), and represents multiple species. However, the depth of groundwater table is pre-set in this approach, which disallows exploration of the impacts of plant water withdrawals on groundwater levels.

Based on this review, a modeling framework explicitly describing the dynamic interactions between the groundwater level and discharge by phreatophytic vegetation can be expected to address a knowledge gap in the literature. Thus, a dynamic groundwater–soil–plant–atmosphere continuum model is proposed here (see Fig. 1). This model combines the hydrodynamics in the saturated and unsaturated zones with leaf-level physiological and soil–root constraints, such that the impacts of capillary rise, hydraulic redistribution, and nocturnal transpiration on the groundwater level are directly considered. The main sources of groundwater recharge or discharge in the proposed model are phreatophytic water withdrawals and the inflow from or outflow to an nearby external water body. In this framework, the groundwater level and root water uptake (i.e., transpiration) are not pre-specified. That is, the predicted groundwater level can be dynamically impacted by transpiration, and vice versa. Specifically, model simulations are used to explore how different plant attributes and environmental factors influence the dynamics of groundwater levels and recharge rates, overall plant transpiration and carbon assimilation, and partitioning of plant water consumption between groundwater and unsaturated soil layers when detailed plant hydraulic processes are included.

2 Model description

The proposed modeling approach is illustrated in Fig. 1, with the notation and units used throughout listed in Table 1. The dynamic groundwater–soil–plant–atmosphere continuum model is developed here by coupling a soil-plant model proposed elsewhere (Huang et al., 2017) with a groundwater balance module. For simplicity, plant water storage is not considered. Information on the formulations and assumptions is given next.

2.1 Leaf gas exchange

A detailed description of the leaf-level gas exchange model included in this work can be found in Huang et al. (2015). Thus, only salient features of the model are summarized here. In this leaf-level gas exchange model, the biochemical demand for CO_2 is described by the Farquhar photosynthetic model for C_3 species (Farquhar et al., 1980). The transfer of CO_2 and water vapor across the stomatal cavity and the laminar boundary layer attached to the leaf surface is modeled as a steady-state Fickian diffusion and constrained by a leaf-level energy balance model to account for the boundary-layer effects (Campbell and Norman, 1998). A residual conductance (g_{res}) is also considered to accommodate the nighttime water leakage through both cuticle and guard cells when nighttime evaporative demand is non-negligible. It is thus suggested that our

model can capture how nocturnal transpiration impacts the groundwater level dynamics when the rooting system is sufficiently deep to reach the groundwater resources. An optimal water use strategy is then used to determine variations in stomatal conductance (g_{s,CO_2}) and subsequently carbon assimilation (f_c) and transpiration (f_e) rates.

2.2 Stomatal closure

Based on the economics of leaf-level gas exchange (Givnish and Vermeij, 1976; Cowan and Farquhar, 1977; Konrad et al., 2008), the optimality hypothesis adopted here to predict g_{s,CO_2} is equivalent to maximizing the objective function defined as:

$$h_a\left(g_{s,CO_2}\right) = f_c - \lambda f_e, \tag{1}$$

where the species-specific parameter λ is known as the marginal water use efficiency that measures the cost of water loss in carbon units. During a dry-down, λ increases on a daily time-scale due to the reduction in available soil water (Manzoni et al., 2013b). The meta-analysis of approximately 50 species (Manzoni et al., 2011) has shown that λ increases as leaf water potential, ψ_l, drops in response to soil drying:

$$\lambda(\overline{\psi}_l) = \lambda^* \frac{c_a}{c_a^*} \exp\left[-\alpha \overline{\psi}_l\right] \tag{2}$$

where λ^* is the minimum water use efficiency under well-watered soil conditions at a reference atmospheric CO_2 concentration $c_a^* = 400$ ppm, $\overline{\psi}_l$ is leaf water potential, ψ_l, averaged over the previous 24-hour period, and α is the species-specific sensitivity parameter. When coupled with the soil-xylem hydraulic system, $\overline{\psi}_l$ is a hydraulic signal representing soil water potential that is not impacted by atmospheric dryness or light variations (Huang et al., 2017; Manzoni et al., 2011). Thus, the predicted g_{s,CO_2} decreases with decreasing $\overline{\psi}_l$ because λ increases as the water availability across the root zone decreases.

2.3 Whole-plant water transport capacity

For the water transport system of vascular plants, the above-ground compartment of the plant xylem water conductance (K) can be described by a vulnerability curve (Huang et al., 2018; Manzoni et al., 2013c):

$$K(\psi_l) = K_{max} \exp\left[-\left(\frac{-\psi_l}{c_1}\right)^{c_2}\right] \tag{3}$$

where K_{max} is the maximum xylem water transport conductance, and c_1 and c_2 are constants describing the shape of K. As soil drought continues, ψ_l becomes more negative in response to the decreasing soil water potential (ψ_s) to maintain f_e. Thus, the linkage between g_{s,CO_2} and the above-ground water transport system can be developed by the supply-demand balance of water (Huang et al., 2018; Manzoni et al., 2014):

$$\begin{aligned} f_{e,s} &= \frac{K(\psi_l)[\psi_{sb} - \psi_l]}{m_v A_l} = \frac{g_{t,H_2O}(e_i - e_a)}{P_a} = f_{e,d} \\ g_{t,H_2O} &= \frac{\left(g_{s,H_2O} + g_{res}\right) g_{b,H_2O}}{g_{s,H_2O} + g_{res} + g_{b,H_2O}} \end{aligned} \tag{4}$$

where $f_{e,s}$ and $f_{e,d}$ are the water supply from above-ground xylem system and the water demand from the atmosphere, respectively; ψ_{sb} is the water potential at the stem base; e_i and e_a are the intercellular and ambient water vapor pressures, respectively; m_v is the molecular weight of

water; A_l is the leaf area; P_a is the atmospheric pressure; g_{t,H_2O} and g_{s,H_2O} ($\sim 1.6 g_{s,CO_2}$) are the total conductance and the stomatal conductance for water vapor, respectively; g_{res} is the residual conductance responsible for water loss through incomplete stomatal closure and cuticle; and g_{b,H_2O} is the boundary layer conductance for water vapor at the leaf scale (Huang et al., 2015). For simplicity, plant water storage is neglected here.

2.4 Water dynamics in the unsaturated zone

The 1-D Richards equation including root water uptake and release (Volpe et al., 2013; Manoli et al., 2014; Bonetti et al., 2015) is used to describe the water transport in the unsaturated soil layer:

$$\begin{aligned} \frac{\partial \theta_s(z_s,t)}{\partial t} &= -\frac{\partial q_s}{\partial z_s} - q_r(z_s,t) \\ q_s &= -K_s(\theta_s)\frac{\partial \psi_s}{\partial z_s} \\ \psi_s &= \phi_s - z_s \end{aligned} \tag{5}$$

where θ_s is the volumetric soil water content at depth z_s below the surface, q_s is the Darcian flux induced by the gradient of total soil water potential ψ_s, q_r is the root water uptake (denoted with superscript '+') or release (denoted with superscript '−') rate, ϕ_s is the soil matric potential, and K_s is the soil hydraulic conductivity. The Clapp and Hornberger formulations (Clapp and Hornberger, 1978) are then used to describe the soil water retention curve and soil hydraulic conductivity function, given by:

$$\phi_s = \phi_{s,sat}\left(\frac{\theta_s}{\theta_{s,sat}}\right)^{-b}, \tag{6}$$

$$K_s = K_{s,max}\left(\frac{\theta_s}{\theta_{s,sat}}\right)^{2b+3}, \tag{7}$$

where $\theta_{s,sat}$, $\phi_{s,sat}$ and $K_{s,max}$ are the soil water content near saturation, the air entry water potential and the saturated hydraulic conductivity, respectively, and b is a constant that varies with soil texture.

In Eq. 5, the change in soil water storage is attributed to the Darcian redistribution (i.e., $-\partial q_s/\partial z_s$) and the water depletion or replenishment rate through the rooting system (i.e., q_r). The q_r is driven by the water potential gradient across the path where water molecules travel radially from the soil to the soil-root interface and the root membrane in series, and is given by:

$$\begin{aligned} q_r &= -k\left[(\psi_{sb} - z_s) - \psi_s\right] a_R \\ k &= \frac{k_r k_s}{k_r + k_s} \end{aligned} \tag{8}$$

where k is the total soil-to-root conductance, $\psi_{sb} - z_s$ is a surrogate for the root water potential (ψ_r), $a_R = 2\pi r B$ is the root surface density, r is the effective root radius, B is the root length density, k_r and $k_s = K_s/l$ are the root membrane permeability and the conductance associated with the radial flow within the soil to the nearest rootlet, respectively, and $l = 0.53/\sqrt{\pi B}$ is the empirical length scale describing the mean radial distance for the movement of water molecules from the soil to the root surface in the rhizosphere (Vogel et al., 2013). We assume here that ψ_r is hydrostatically distributed (i.e., $\psi_r = \psi_{sb} - z_s$) because the water storage and energy losses are negligible within the roots (Lafolie et al., 1991; Siqueira et al., 2008) when compared to the above-ground compartments (Kavanagh et al., 1999).

In the absence of plant water storage, the coupling of the rooting system with the above-ground plant system can be described by the supply-demand balance for water between net root water uptake (RWU_{net}) and total transpiration rate (F_e):

$$F_e = f_e m_v A_l = RWU_{net} = \left[\int_{L_R}^{0} (q_r^+ + q_r^-) dz_s\right] \rho A_{soil} \tag{9}$$

where L_R is the rooting depth, ρ is the water density, and A_{soil} is the soil surface area covering the roots. Thus, $Q_{r,s} = \left(\int_{L_R}^{y} q_r^+ dz_s\right) \rho A_{soil}$ and $Q_{r,us} = \left(\int_{y}^{0} q_r^+ dz_s\right) \rho A_{soil}$, where y is the groundwater depth, are the total root water uptake from the saturated and unsaturated zones, respectively. During daytime, a significant water potential gradient from roots to leaves can drive root water uptake (i.e., q_r^+) for all z_s when transpiration is large. However, root water uptake from lower soil columns (i.e., saturated and unsaturated zones) can be released back to dryer soil layers and contributes to transpiration when transpiration is small. During nighttime, root water uptake from the lower saturated zone can be released back to the upper saturated zone (causing rise of y) and dry soil layers. That is, the rooting system (compared to soil medium) becomes a highway to transport water between soil layers in the presence of soil water potential gradient during the night. Here, hydraulic redistribution (HR) is defined as the water release to the unsaturated zone and computed as $Q_{r,us}^- = |\left(\int_{y}^{0} q_r^- dz_s\right) \rho A_{soil}|$.

2.5 Groundwater dynamics

The water balance in the saturated zone (i.e., groundwater) is given as (Laio et al., 2009; Ridolfi et al., 2008):

$$\beta(y(t)) \frac{dy(t)}{dt} = O_{in} - Q_{r,s} - E_x \tag{10}$$

where β is the specific yield representing the volume of water gain or loss due to the rise or fall of a water table, O_{in} is the inflow (+) from or outflow (−) to the external water body depending on the relative depths between groundwater and external water body, and E_x is the exfiltration rate driven by capillary rise. In Eq. 10, the groundwater dynamics (i.e., y) are impacted by both F_e and HR through the sink term, $Q_{r,s}$. To predict y, O_{in} and E_x require specification, which is discussed next.

2.5.1 Recharge or discharge through a nearby water body

The lateral flow into or out of the groundwater underneath a horizontally uniform vegetation (i.e., recharge or discharge) is driven by the presence of an external water body in the proposed modeling framework (Fig. 1). When the water level of the external water body (y_0) is a constant in time and the distance between the external water body and vegetated area is sufficiently large, the inflow or outflow rate from the external water body, O_{in}, can be described by the linear reservoir approximation based on Darcy's law (Laio et al., 2009; Ridolfi et al., 2008):

$$\begin{aligned} O_{in} &= K_g(y_0 - y) \\ K_g &= \tfrac{K_s}{L_s + y} \end{aligned} \tag{11}$$

where L_s is the distance between the soil surfaces at the vegetated area and under the external water body, and K_g is a constant depending on the soil properties (i.e., K_s) and the transport distance from or to the external water body (i.e., $L_s + y$). While $|y_0| < |y|$ leads to a recharge (i.e., $O_{in} > 0$), a discharge (i.e., $O_{in} < 0$) is guaranteed for $|y_0| > |y|$. Moreover, the total water

potential for the groundwater layer under the vegetated area, H, is linearly distributed in the vertical direction:

$$H = \underbrace{z_s}_{\text{Elevation head}} \quad \underbrace{-(1+C)z_s + y_0 - CL_s}_{\text{Pressure head}}, \tag{12}$$

where $C = O_{in}/K_s$ is the normalized recharge or discharge rate. It should be noted that the dynamic variation of H (i.e., not hydrostatic) can impact the water potential in the rooting zone and subsequently F_e and HR (a hydrostatic condition is not assumed here).

2.5.2 Capillary rise

Capillary rise (i.e., exfiltration rate) is the upward movement of pore water driven by the gradient in hydraulic head. In the presence of groundwater, E_x (see Eq. 10) represents the upward water flux from saturated zone to neighboring unsaturated infinitesimal soil layer, and can be approximated by a Darcian flux (Gardner, 1958; Lu and Likos, 2004):

$$E_x = q_s|_{z_s = y + \delta z_s} \tag{13}$$

where δz_s is the depth of the unsaturated infinitesimal soil layer right above y. When formulated in this manner, E_x is represented as the tendency for the neighboring unsaturated soil layer to reach a hydrostatic condition after root water uptake (i.e, q_r). Thus, E_x can be impacted by the antecedent water status in δz_s through F_e and HR.

2.6 Model set-up

Nine scenarios were constructed to explore how different environmental conditions and plant attributes impact the dynamic interactions between the groundwater level and phreatophytic vegetation (see Table 2) when y_0 is fixed as a constant (i.e., 0.75 m below the surface) and the initial y was set equal to y_0 across all scenarios. The main source responsible for recharge is the nearby external water body (i.e., no precipitation). Since it is difficult to obtain the plant physiological, hydraulic attributes from a single experiment, the plant model parameters were collected from the literature with a focus on *Pinus taeda* L. When parameters specific for *Pinus taeda* L. were not available, parameters for coniferous species in general and pine plantation trees were adopted (see Huang et al. (2017) for detailed information) for all model runs. It should be also noted that *Pinus taeda* L. is a phreatophytic plant with accessibility to shallow groundwater in Southeastern USA (Aguilos et al., 2021; Wahlenberg et al., 1960). For the soil hydraulic parameters, the required parameters in Eq. 6 and 7 were adopted from Clapp and Hornberger (1978). The model parameterizations are summarized in Appendix A. The bottom of the domain in the modeling system was considered as a no-flow boundary in all simulations (Loheide et al., 2005). The vertical discretization of soil domain and time step were set as 0.075 cm and 0.02 s, respectively. For all model runs, the initial soil water conditions were specified as hydrostatic for the unsaturated zone. The model calculations were subsequently repeated with prescribed atmospheric variables on a periodic 24-h basis and that drove the dynamic groundwater-phreatophyte interactions (see Appendix). All the model runs were simulated for 15 days to ensure that the daily equilibrium state can be captured.

In S1-S3, we set leaf area index (LAI) = 1.5 m^2 m^{-2}, g_{res} = 0.04 mol m^{-2} s^{-1}, and a rooting depth of 1.2 m. The soil type was set as clay to represent finer soil particles with a small K_s as listed elsewhere (Clapp and Hornberger, 1978). When all other model parameters and environmental conditions remained the same, reverse power-law ($B = B_{RP}$), power-law ($B = B_P$) and uniform root distributions ($B = B_U$) were set in S1, S2 and S3 (see Fig.

2), respectively. Thus, the impacts of vertical root distribution can be explored through the comparison between S1, S2 and S3 as the total root length densities across all the scenarios were maintained the same ($\sim 1 \times 10^7$ m m^{-3}). The setup for S2 here is used to represent *Pinus taeda* L. following a power-law rooting distribution common for many species including coniferous species (Andersson, 2005; Finér et al., 1997; Jackson et al., 1996). A reverse power-law distribution has been observed for plants in contact with the groundwater such as *Prosopis glandulosa* var. Torreyana (Jarrell and Virginia, 1990) and can be also used to represent plants with only sinker roots extending into groundwater such as *Celtis* as reported by Hultine et al. (2003). Since LAI and g_{res} are finite and the rooting system can reach the groundwater, both F_e (i.e., daytime and nocturnal) and HR can directly modify the dynamic y.

Regarding leaf attributes, S4 used a larger LAI (3 m^2 m^{-2}) and S5 adopted a smaller g_{res}. The values of g_{res} (0.01 and 0.04 mol m^{-2} s^{-1}) used here were well within the range for many species reported elsewhere (Caird et al., 2007). To explore how soil texture impacts the groundwater-phreatophyte interactions, the soil type in S6 was modified to clay loam such that the K_s is nearly doubled when compared to clay as listed elsewhere (Clapp and Hornberger, 1978). Scenarios S7-S9 focused on the impact of changing environmental conditions. In S7, we increased CO_2 concentration from 400 to 500 ppm and in S8, we increased air temperature by 1.5 ^{o}C following the upper boundary of the indicative likely range for all RCP scenarios at the end of 2035 (IPCC, 2013). In S9, the CO_2 concentration and air temperature were simultaneously increased to explore their combined effects on the groundwater level. When air temperature is increased in S8 and S9, actual vapor pressure varies with saturation vapor pressure assuming relative humidity is not sensitive to changes in air temperature (Katul et al., 2012).

3 Results and discussion

To address the study objectives, we first analyze how soil water dynamics are impacted by daytime and nocturnal F_e and HR in Section 3.1. In Section 3.2, how the diurnal fluctuations of y are generated in relation to daytime and nocturnal F_e (i.e., $Q_{r,s}$) and HR as well as O_{in} is then discussed. When roots can directly utilize groundwater resources, we examine the sensitivity of leaf-level responses to different root distributions, soil textures, leaf attributes and future climate conditions in Section 3.3. In Section 3.4, how the total plant water use ($Q_r = Q_{r,s} + Q_{r,us}$) is partitioned to $Q_{r,s}$ and $Q_{r,us}$ and its relation to the fraction of roots submerged in groundwater (R) across all scenarios is presented. Based on the results from the proposed modeling approach and previous studies, how the accessibility of groundwater to the rooting system impacts the magnitude of HR is discussed in Section 3.5. The mechanisms leading to changes in y across all scenarios are explained in Section 3.6. Finally, a brief summary of the study limitation in the present modeling framework is presented in Section 3.7. To maintain a minimum number of scenarios, the discussion here is based on the comparison to S1 when only one parameter in each scenario (i.e., S2-S9) is modified.

3.1 General features of the modeled soil water dynamics

The modeled profiles of diurnal variations in θ_s and q_r across L_R are shown in Fig. 3(a) and (b), respectively, for S1. When light activates photosynthesis during the day, phreatophytes begin to extract water from both the unsaturated and saturated zones (i.e., $F_e > 0$), thereby reducing θ_s of the upper soil layer and y. However, the plant water consumption from the saturated zone is much larger than that from the unsaturated zone. This can be explained by the fact that 1) the majority of the roots are located below the groundwater level and 2) root water uptake is

higher when water potential is near zero in the saturated zone. When light diminishes to zero at night, a finite $Q_{r,s}$ is still maintained. This nocturnal $Q_{r,s}$ contributes to both nocturnal F_e and HR (i.e., $Q^-_{r,us}$). Therefore, the upper soil layers can be partially refilled by HR, but the rise of y is still limited by nocturnal $Q_{r,s}$. This suggests that the assumption of negligible plant groundwater usage at night is not valid when applying WM to estimate groundwater consumption by phreatophytes.

We should also emphasize that nocturnal F_e can suppress HR (Howard et al., 2009; Hultine et al., 2003; Prieto et al., 2010; Scholz et al., 2008) although it can limit the rise of y at night. Nocturnal F_e is inevitable water loss through incomplete stomatal closure and cuticle (i.e., embedded in g_{res}) at the leaf level and is not regulated by photosynthesis (Boyer et al., 1997; Larcher, 2003). Thus, nocturnal F_e is governed primarily by the magnitude of g_{res} and the atmospheric dryness (e.g., vapor pressure deficit, D) (Domec et al., 2012a), not the soil water status as L_R can reach the saturated zone. Moreover, nocturnal F_e generates a residual water potential gradient along the plant vascular system during the night. Such non-negligible competing sink strength can further reduce the magnitude of HR (Huang et al., 2017) when HR is driven by the water potential gradient across L_R to move water from the saturated to the unsaturated zone (Neumann and Cardon, 2012). This suggests that a larger nocturnal F_e does not guarantee a smaller rise of y at night because HR is simultaneously reduced. Unlike nocturnal F_e, it should be noted that the water redistributed to the unsaturated zone through HR can be later used by plants (Warren et al., 2007). Furthermore, HR can also maintain root hydraulic conductivity and microbial activity, enhance nutrient uptake through maintaining soil–root contact in the unsaturated zone, and deliver water to neighboring species with shallower rooting depth (Brooks et al., 2006; Domec et al., 2004; Prieto et al., 2012).

3.2 General features of the modeled groundwater level and recharge rate

Fig. 4 showcases the general predicted dynamics of y, $Q_{r,s}$, F_e and O_{in} using S1 as an example. The diurnal fluctuations of y and O_{in} occur due to the presence of groundwater consumption through plants (i.e., $F_e \neq 0$ and $Q_{r,s} \neq 0$). The predicted difference between daily maximum and minimum y (~ 0.05 m) is well within the range of 0.01-0.6 m as reported elsewhere (Carlson Mazur et al., 2014b; Cooper et al., 2006; Crosbie et al., 2019; Fahle and Dietrich, 2014; Gribovszki et al., 2008; Gribovszki, 2018; Healy and Cook, 2002; Lautz, 2008; Loheide et al., 2005) with similar patterns of diurnal fluctuations of y. At the beginning of the simulation, $y = y_0 = 0.75$ m leads to $O_{in} = 0$. When light activates photosynthesis, y decreases because $Q_{r,s} > 0$ driven by plant groundwater consumption through daytime transpiration ($F_e > 0$) is larger than $O_{in} \sim y_0 - y > 0$ (see Eq. 11). When F_e recedes to a minimum during nighttime, $O_{in} > Q_{r,s}$ leads to an increase in y. However, nocturnal $Q_{r,s}$ is not negligible in the presence of HR and nocturnal F_e (see Section 3.1). It should be noted that $y \sim y_0$ with $O_{in} \sim 0$ requires $Q_{r,s} \sim 0$. Thus, $y < y_0$ (i.e., $O_{in} > 0$) is guaranteed when plant groundwater consumption (i.e., daytime and nocturnal F_e) and water movement through the rooting system (i.e., HR) continues. That is, the daily variation in O_{in} is also dictated by y through changes in $Q_{r,s}$. This further suggests that the assumption of a constant O_{in} during a daily cycle in the WM is not valid when phreatophytic plants can modify y and subsequently $Q_{r,s}$.

3.3 Stomatal responses to variations in plant attributes and environmental conditions

Fig. 5 shows comparisons of g_{s,CO_2}, f_e and f_c for all scenarios. The predicted g_{s,CO_2}, f_e and f_c remain similar when root distributions (S1, S2 and S3) and soil properties (S1 and

S6) are modified. These results may not be surprising since water availability is not limiting stomatal responses for any cases. Groundwater accessibility by the rooting systems and a moist unsaturated zone due to HR guarantee sufficient water supply to maintain g_{s,CO_2}. This explains why different root distributions and soil properties do not appreciably impact g_{s,CO_2} as well as f_e and f_c as long as the total root densities remain the same.

However, g_{s,CO_2}, f_e and f_c vary with different leaf attributes (S1, S4 and S5) and atmospheric conditions (S1, S7, S8 and S9). A larger LAI in S4 increases total evaporative demand (i.e., F_e) such that the water availability in the unsaturated zone and the root fraction submerged in the saturated zone (R) are reduced. Thus, the overall water availability across the root zone in S4 decreases, thereby generating smaller g_{s,CO_2}, f_e and f_c in comparison to S1. Contrarily, a larger g_{s,CO_2} is predicted by reductions in f_e with a reduced g_{res} (S5) when compared to S1. A smaller g_{res} in S5 reduces evaporative demand (i.e., f_e) but maintains a greater overall water availability with a larger R.

Regarding the impacts of atmospheric conditions on g_{s,CO_2}, the proposed model predicts a smaller g_{s,CO_2} in S7 with increasing c_a and a larger g_{s,CO_2} in S8 with increasing T_a when compared to S1. The overall trends in negative response to increasing c_a and positive response to increasing leaf temperature (T_l) are mainly reflected by the supply-demand balance of CO_2 flux (Huang et al., 2018) and have been reported elsewhere (Mansfield et al., 1990; Messinger et al., 2006; Morison, 1998; Morison and Gifford, 1983; Mott, 1988). Specifically, increasing temperature generally enhances photosynthetic capacity and subsequently stomatal conductance. In some ecosystems, however, temperature may be already close to or above the thermal optimum so that warming inhibits (rather than promotes) photosynthesis (Dusenge et al., 2019). It should be also noted that increasing T_a in S8 not only generates a larger leaf temperature, T_l, but also a larger D. Their combined effects on g_{s,CO_2} cannot be separated. The negative trends in g_{s,CO_2} with respect to increasing D have been widely reported (Aphalo and Jarvis, 1991; Grantz, 1990; Katul et al., 2009; Lendzion and Leuschner, 2008; Massman and Kaufmann, 1991; McAdam and Brodribb, 2015; Monteith, 1995; Oren et al., 1999).

However, a positive response of g_{s,CO_2} to increasing T_a is produced because the degree of increasing g_{s,CO_2} induced by increasing T_l (due to a higher rate of photosynthesis) overshadows the negative response due to increasing D in the case of S8. When c_a and T_a are simultaneously increased to represent future climate regime (i.e., S9), the model result here suggests that the reduction in g_{s,CO_2} in response to increasing c_a (i.e., S7) roughly compensates the effects of hotter and drier atmospheric condition on g_{s,CO_2} (i.e., S8). Thus, the consideration of both increasing c_a and T_a generates a greater water use efficiency (i.e., f_c/f_e) in S9 where f_c is largely enhanced but f_e does not appreciably increase. It should be also noted that how f_e is impacted by the opposing effects from increasing T_a and c_a largely depends on their degrees of increases and the species considered (Kirschbaum and McMillan, 2018).

3.4 Partitioning of plant water use between saturated and unsaturated zones

Across all scenarios, the modeled fraction of root water uptake from the saturated zone ($Q_{r,s}/Q_r$) increases linearly with increasing root fraction submerged in the groundwater (R) (see Fig. 6(a)). Thus, the partitioning of plant water use between the saturated and unsaturated zones is mainly dictated by the root distribution. Examining the model results of S1, S2 and S3 for different root distributions, it is evident that R determines the $Q_{r,s}/Q_r$ even when F_e remains similar. The magnitude of F_e can also largely impact $Q_{r,s}/Q_r$ and R when the root distribution stays the same. For instance, a larger $Q_{r,s}$ induced by a larger F_e in S4 with a doubled LAI creates a deeper y that generates a smaller R and $Q_{r,s}/Q_r$ in comparison to S1. The model results here also suggest that groundwater (not unsaturated zone) is the main water supply to phreatophytes

across all scenarios. For example, the predicted $Q_{r,s}/Q_r$ can be larger than 80% when R is only 60 to 70 %. When R is only $\sim 9\%$, $Q_{r,s}$ can still contribute to more than 30% of Q_r.

The daily total $Q_{r,s}$ across all scenarios and the ratio between nighttime $Q_{r,s}$ and daily total $Q_{r,s}$ are shown in Fig. 6(b) and (c), respectively. While the daily total $Q_{r,s}$ is mainly governed by the daily total F_e and R, the nighttime $Q_{r,s}$ contributes to both HR and nocturnal F_e. Comparing the impact of root distribution on $Q_{r,s}$ in S1, S2, and S3 shows that the largest R in S1 generates the largest daily total $Q_{r,s}$ with a similar F_e. When leaf area is increased in S4, a larger F_e generates a larger daily total $Q_{r,s}$. When leaf area is maintained the same, the magnitude of F_e simply varies with the transpiration rate per unit leaf area (i.e., f_e). Consequently, the trend in the daily total $Q_{r,s}$ follows the trend in f_e (see Fig. 5(b)) across S1, S5, S6, S7, S8 and S9. For instance, a larger atmospheric CO_2 concentration in S7 reduces F_e such that the daily total $Q_{r,s}$ in S7 becomes smaller than the case of S1. Furthermore, the predicted ratio between nighttime $Q_{r,s}$ and daily total $Q_{r,s}$ ranges from 11.6 to 21.4 %. Again, the modeled results here suggest that negligible nighttime plant groundwater usage as assumed in WM is not valid. Since nocturnal F_e remains similar across scenarios (i.e., same g_{res}) except for S5 with a much smaller F_e (i.e., smaller g_{res}), how nighttime $Q_{r,s}$ varies with different scenarios is mainly determined by their magnitudes of HR as discussed next.

3.5 Model analysis for hydraulic redistribution (HR)

In Fig. 7, the comparison of daily averaged HR for all scenarios is illustrated. The accessibility of groundwater to the rooting system can impact the magnitudes of HR for different root distributions. When roots are far from the groundwater, previous experiments and modeling studies have shown that a vertically asymmetric root distribution corresponds to an increased HR (Huang et al., 2017; Scholz et al., 2008; Siqueira et al., 2008; Volpe et al., 2013). A larger soil water potential gradient created by the asymmetric root distribution during daytime transpiration facilitates a greater HR at night (Huang et al., 2017). When roots are able to continuously access groundwater, however, a smaller HR is predicted here for a vertically asymmetric root distributions compared with its uniform counterpart (see Fig. 7(a)). A pattern similar to the model predictions has been reported for three desert phreatophytic plants (Hultine et al., 2003). When *Fraxinus* and *Juglans* exhibit dimorphic root distributions with a network of shallow lateral roots and deep taproots down to the water table, their root distributions can be approximately represented as uniform root distribution across both saturated and unsaturated zone in S3. When *Celtis* has only sinker roots extending into groundwater, the reverse power-law root distribution with root density concentrated within groundwater in S1 can be used to represent its rooting system. Interestingly, reverse sap flow in roots (i.e., evidence of HR) was observed for *Fraxinus* and *Juglans* but no HR was found for *Celtis*. This suggests that the water potential gradient alone is not sufficient to drive HR. A sufficient number of roots across the root zone in both the saturated and unsaturated zones is another key factor facilitating HR (see Eq. 8).

As discussed in Section 3.1, the residual water potential gradient along the plant vascular system created by the nocturnal evaporative demand (i.e., nocturnal F_e) can diminish HR. This explains why the modeled HR's in S4 and S5 are respectively smaller and larger than that in S1 (Fig. 7(b)). When compared with S1, nocturnal F_e increases with increasing LAI in S4, but decreases with a smaller g_{res} in S5. Regarding soil texture, the comparison between S1 and S6 suggests that coarser-textured (i.e., larger K_s) soils result in a smaller intensity of HR compared with finer-textured counterpart (Fig. 7(c)). A split-root experiment (Wang et al., 2009) and the experiments conducted in the Mojave Desert (Yoder and Nowak, 1999) have reported such a trend associated with the impact of soil texture on HR. However, the mechanism leading to such a similar trend is different from the model simulation here because their rooting systems are

not in contact with groundwater. When roots are far from the groundwater, the development of the soil water potential gradient required for HR is hindered by rapid drainage for the case of coarser-textured soils (Burgess et al., 2000; Scholz et al., 2008). When roots can reach the groundwater as the cases explored here, coarser-textured soil in S6 promotes the daytime use of water from unsaturated soil layers per unit depth. Thus, coarser-textured soils create a shallower daytime y, resulting in a smaller number of roots in the unsaturated soil domain (see Fig. 6(a)) for the development of HR at night. Again, the number of roots needs to be sufficiently large in both the saturated and unsaturated zones to drive HR, as discussed for the three cases with different root distributions (i.e., S1, S2 and S3).

How future climate conditions can potentially impact the magnitude of HR with roots in contact with groundwater is explored here by comparing S7, S8 and S9 with S1 (Fig. 7(d)). The proposed model predicts a larger HR with elevated c_a (i.e., S7) and a smaller HR with increasing T_a (i.e., S8) when compared to S1. F_e in S7 is reduced by the reduction in g_{s,CO_2} as discussed in Section 3.3. S7 then creates a slightly shallower y (i.e., smaller a_R in the unsaturated zone) and a wetter unsaturated soil zone (i.e., larger k and less negative ψ_s) in comparison to S1. The positive response of HR to an increasing c_a is predicted here because the degree of increasing k overshadows the combined effects of increased ψ_s and decreased a_R in the unsaturated zone (see Eq. 8). However, we should also stress that such a positive response of HR to an increasing c_a only occurs when y and a_R in the unsaturated zone are not appreciably modified, as is the case here. HR can be significantly suppressed if a_R in the unsaturated zone is largely reduced due to the rise of y. The increase in T_a (i.e., S8) enhances daytime F_e that generates a greater water potential gradient across the root zone to drive HR. However, nocturnal F_e also increases with increased T_a (i.e., D) such that HR is further suppressed by the residual water potential gradient along the vascular system. Interestingly, one previous modeling approach (Volpe et al., 2013) reported an opposite trend for the case of roots far from groundwater table. An increased c_a produces a reduction in HR because of reductions in root water uptake and water potential gradient across the root zone when roots are not in contact with groundwater. The reason that enhancement in HR with an increased T_a is predicted by Volpe et al. (2013) is because g_{res} is not considered. Thus, nocturnal F_e is absent in their model to diminish HR. Simultaneously considering increased c_a and T_a to represent the future climate regime (i.e., S9), the model result here suggests that the increase in HR in response to elevated c_a (i.e., S7) compensates the effects of increased T_a on HR (i.e., S8).

3.6 Model analysis for groundwater level

The modeled daily averaged y's and nighttime rise in y's for all scenarios are shown in Fig. 8 and 9, respectively. Regarding different root distributions (i.e., S1, S2, and S3) (Fig. 8 (a)), daily averaged y's are determined by $Q_{r,s}/Q_r$ and the magnitudes of HR because their F_e's remain similar (see Section 3.3). When R is only $\sim 9\%$ for the case of power-law distribution (i.e., S2), the water withdrawal from the saturated zone (i.e., $Q_{r,s}/Q_r$) is reduced (see Fig. 6). Thus, the daily averaged y becomes shallower and nighttime rise of y in S2 becomes smaller (Fig. 9) when compared with S1 (i.e., $R \sim 62\%$). Considering the case of uniform root distribution (i.e., S3), its daily averaged y is predicted to be similar to S1 with a reverse power-law distribution. Indeed, the daytime drop in y for S3 is smaller than that for S1 (see inset in Fig. 8 (a)), given that R and $Q_{r,s}/Q_r$ are largely reduced (see Fig. 6). However, a smaller rise in nighttime y (Fig. 9) caused by a larger HR in S3 (see Section 3.5) further reduces the difference in daily averaged y between S1 and S3.

Since y is mainly controlled by $Q_{r,s}$ (see Section 3.2), the magnitudes of F_e modified by different leaf attributes (i.e., S1, S4, and S5) and atmospheric conditions (i.e., S1, S7, S8, and

S9) can directly impact y through changes in $Q_{r,s}$. An increased $Q_{r,s}$ caused by a larger F_e generates a deeper y and a larger nighttime rise in y (i.e., a larger recharge rate). When comparing y's for different leaf attributes (Fig. 8 (b)), a deeper y in S4 than in S1 is predicted when F_e is largely enhanced by an increase in LAI. Contrarily, $Q_{r,s}$ is reduced by a smaller g_{res} (i.e., S5 with a smaller F_e) (Huang et al., 2015) leading to a shallower y in S5 than in S1. Considering the potential impacts of future climate conditions on y (Fig. 8 (d)), y increases with an elevated c_a (i.e., S7; decreased F_e and $Q_{r,s}$) but deceases with an increased T_a (i.e., S8; increased F_e and $Q_{r,s}$). Again, the combined effects of elevated c_a and increasing T_a on y (i.e., S9) may be negligible when F_e (i.e., $Q_{r,s}$) is not appreciably modified as the case here (see Section 3.3).

When compared with different soil properties (i.e., S1 and S6), the proposed model predicts a shallower daily averaged y for coarser-textured soil with a larger K_s (Fig. 8 (c)). A pattern similar to the modeled results here has been also reported by a previous modeling study using four different soil textures (Loheide et al., 2005). The drop in daytime y decreases with an increased daytime use of water from unsaturated soil layers for the coarser-textured soil. Moreover, a suppressed HR due to a shallower daytime y (see Section 3.5) further reduces the rise in y at night (Fig. 9), resulting in an overall shallower daily averaged y.

3.7 Study limitations

Given all the assumptions taken to arrive at the proposed model, it is informational to recapitulate its limitations for future improvements. Modeling uncertainties can be further reduced when the relative humidity in the leaf inter-cellular spaces and plant water storage are appropriately described. Recent studies have suggested that the water vapor inside the stomatal cavity may not be saturated especially when the surrounding air is dry (Cernusak et al., 2018, 2019; Wong et al., 2022). Thus, the assumption of saturated water vapor inside the stomatal cavity at T_l here may overestimate the evaporative demand, impacting the dynamics of modeled g_{s,CO_2} and y. The presence of plant water storage can reduce y because it represents an above-ground reservoir to store groundwater. However, plant water storage can also reduce root water uptake and HR at night (Huang et al., 2017). Thus, the degree of impact on y through plant water storage depends on the overall water storage capacity in the targeted ecosystem and requires further exploration. The proposed model also assumes that the lateral inflow from an external water body is the main source to recharge the groundwater. However, different geometries of the flow system can result in different dynamics of y (Loheide et al., 2005). Moreover, uncertainties in modeling y can be further reduced when the spatiotemporal dynamics of below-ground root distribution, above-ground plant structure and their hydraulic and physiological attributes are appropriately described. For instance, all the aforementioned properties can vary under future climate conditions. Horizontal heterogeneity in root distribution and plant structure at the landscape scale also needs to be further accounted for. Lastly, phreatophytic vegetation with a deeper rooting depth and y (e.g., > 2 m) is not uncommon (Butler Jr et al., 2007; Canham et al., 2012; Hultine et al., 2003; Wang et al., 2021). In such a case of y further away from the surface, the soil water status in the upper soil layer and the magnitude of HR may not be maintained at the same level as the case of shallow y. Thus, additional field and modeling experiments are required to further understand the dynamic fluctuation of y in relation to the responses of phreatophytic vegetation for a deeper y.

4 Conclusions

The main goal of this work was to further understand the dynamic interactions between groundwater level and discharge by phreatophytic plants without invoking the *ad hoc* assumptions adopted by the White method. To address this goal, we developed a dynamic groundwater–soil–plant–atmosphere continuum model to describe the water dynamics throughout the saturated and unsaturated soil domain as well as soil-root interface and plant vascular system. When HR and nocturnal F_e are also considered, y and Q_r can dynamically interact with each other in the resulting modeling approach. Based on model results for a broad range of environmental conditions and plant attributes, a number of conclusions can be drawn:

1) The assumptions of negligible plant groundwater usage during the night and a constant O_{in} in White method may not always occur in natural settings. Although HR is limited by nocturnal F_e through a residual water potential gradient along the plant vascular system, both HR and nocturnal F_e are able to reduce y at night. The fluctuation in y caused mainly by the diurnal variation of F_e further suggests that O_{in} cannot be constant (i.e., $O_{in} \sim y_0 - y > 0$) as in the cases explored here.

2) Since the model simulations here consider the cases of rooting system in contact with shallow groundwater (i.e., $y > -1$ m), the leaf-level gas exchange operates with little to no limitation of water supply. Thus, g_{s,CO_2}, f_e and f_c are not appreciably impacted by different root distributions or soil textures, but they still vary with various atmospheric conditions as if the soil domain is under a well-watered condition. This explains why the correlation between y and leaf-level gas exchange across all the scenarios explored here is weak. However, $Q_{r,s}/Q_r$ linearly increases with increasing R as y increases.

3) In the scenarios represented here which describe shallow groundwater levels, a sufficient volume of roots connecting the saturated and unsaturated zones becomes the dominant factor driving HR, rather than the water potential gradient across the rooting depth. Thus, the impact of y on the partitioning of root volume between saturated and unsaturated zone for different root distributions determines the magnitude of HR. This explains why a vertically asymmetric root distribution does not guarantee enhancement in HR and HR is reduced by coarser-textured soils with a shallower y.

4) Exogenous environmental factors (e.g., soil texture and atmospheric conditions) and endogenous plant properties (e.g., root distribution and leaf attributes) can impact the dynamics of y through modifications in $Q_{r,s}$ and HR. Interestingly, the proposed modeling approach predicts that y may not be appreciably impacted by simultaneous increases in c_a and T_a when F_e (i.e., $Q_{r,s}$) remains similar under future climate regime. However, the water use efficiency is enhanced as f_c increases with an elevated c_a.

Acknowledgments

Support from the Department of Energy (DOE) through the Office of Biological and Environmental Research (BER) (DE-SC0023468) and the National Science Foundation (NSF-CBET-2139003) is acknowledged.

List of Tables

1. Nomenclature

2. Nine scenarios (S1-S9) set up to explore dynamic interactions between groundwater and phreatophytes

Table 1: Nomenclature

Symbol	Description	Unit
A_l	Leaf area	m^2
A_{soil}	Soil surface area covering the roots	m^2
a_R	Root surface density	$\mathrm{m^2 m^{-3}}$
B	Root length density	$\mathrm{m\ m^{-3}}$
b	Empirical constant for soil water retention curve and hydraulic conductivity function	Dimensionless
C	Normalized recharge or discharge rate($= O_{in}/K_s$)	$\mathrm{kg\ m^{-1}}$
c_a	Atmospheric CO_2 concentration	ppm
c_a^*	Reference atmospheric CO_2 concentration ($= 400$)	ppm
c_1	Constant describing the shape of K	MPa
c_2	Constant describing the shape of K	Dimensionless
E_x	Exfiltration rate	$\mathrm{kg\ s^{-1}}$
e_a	Ambient water vapor pressures	kPa
e_i	Inter-cellular water vapor pressures	kPa
F_e	Total transpiration rate ($= f_e m_v A_l = RWU_{net}$)	$\mathrm{kg\ s^{-1}}$
f_c	Assimilation rate per unit leaf area	$\mu\mathrm{mol\ m^{-2}\ s^{-1}}$
f_e	Transpiration rate per unit leaf area	$\mathrm{mol\ m^{-2}\ s^{-1}}$
$f_{e,s}$	Water supply function	$\mathrm{mol\ m^{-2}\ s^{-1}}$
$f_{e,d}$	Water demand function	$\mathrm{mol\ m^{-2}\ s^{-1}}$
g_{s,CO_2}	Stomatal conductance	$\mathrm{mol\ m^{-2}\ s^{-1}}$
g_{t,H_2O}	Total conductance for water vapor	$\mathrm{mol\ m^{-2}\ s^{-1}}$
g_{s,H_2O}	Stomatal conductance for water vapor ($\sim 1.6 g_{s,CO_2}$)	$\mathrm{mol\ m^{-2}\ s^{-1}}$
g_{res}	Nocturnal residual conductance	$\mathrm{mol\ m^{-2}\ s^{-1}}$
g_{b,H_2O}	Boundary layer conductance for water vapor	$\mathrm{mol\ m^{-2}\ s^{-1}}$
h_a	Objective function	$\mu\mathrm{mol\ m^{-2}\ s^{-1}}$
K	Plant xylem water conductance	$\mathrm{kg\ s^{-1}\ MPa^{-1}}$
K_{max}	Maximum xylem water transport capacity	$\mathrm{kg\ s^{-1}\ MPa^{-1}}$
K_s	Soil hydraulic conductivity	$\mathrm{m\ s^{-1}}$
$K_{s,max}$	Saturated soil hydraulic conductivity	$\mathrm{m\ s^{-1}}$
K_g	Constant depending on K_s	$\mathrm{s^{-1}}$
k	Total soil-to-root conductance	$\mathrm{s^{-1}}$
k_r	Root membrane permeability	$\mathrm{s^{-1}}$
k_s	Conductance associated with the radial rootlet flow within the soil to the nearest rootlet	$\mathrm{s^{-1}}$
LAI	Leaf area index	$\mathrm{m^2\ m^{-2}}$
L_R	Rooting depth ($= 1.2$)	m
L_s	Distance between the soil surfaces at the vegetated area and under the external water body ($= 5$)	m
l	length scale describing the mean radial distance for the movement of water molecules from the soil to the root surface in the rhizosphere	m
m_v	Molecular weight of water	$\mathrm{kg\ mol^{-1}}$
O_{in}	Inflow (+) from or outflow (−) to the external water body	$\mathrm{kg\ s^{-1}}$
P_a	Atmospheric pressure	kPa
$Q_r = Q_{r,s} + Q_{r,us}$	Total plant water use	$\mathrm{kg\ s^{-1}}$
$Q_{r,s}$	Total root water uptake from saturated zone	$\mathrm{kg\ s^{-1}}$

Continued on next page

Table 1 – continued from previous page

Symbol	Description	Unit
$Q_{r,us}$	Total root water uptake from unsaturated zone	kg s^{-1}
$Q^{-}_{r,us}$	Hydraulic redistribution	kg s^{-1}
q_s	Darcian flux	m s^{-1}
q_r	Root water uptake/release per unit soil volume	s^{-1}
RWU_{net}	Net root water uptake across the root zone	kg s^{-1}
R	Fraction of roots submerged in groundwater	Dimensionless
r	Effective root radius	m
t	Time	s
y	Groundwater depth	m
y_0	Water level of external water body	m
z_s	Depth below the surface	m
δz_s	Depth of the unsaturated infinitesimal soil layer right above y	m
λ	Marginal water use efficiency	μmol mol^{-1} kPa^{-1}
λ^*	Marginal water use efficiency under well-watered soil conditions	μmol mol^{-1} kPa^{-1}
α	Species-specific sensitivity parameter	MPa^{-1}
β	Specific yield	kg m^{-1}
ψ_l	Leaf water potential	MPa
ψ_r	Root water potential	MPa
ψ_s	Total soil water potential	m
$\psi_{s,b}$	Water potential at the stem base	MPa
ϕ_s	Soil matric potential	m
$\phi_{s,sat}$	Soil air entry water potential	m
$\overline{\psi}_l$	ψ_l averaged over the previous 24 hours period	MPa
θ_s	Volumetric soil water content	m^3 m^{-3}
$\theta_{s,sat}$	Soil water content near saturation	m^3 m^{-3}
ρ	Density of water	kg m^{-3}

Table 2: Nine scenarios (S1-S9) set up to explore dynamic interactions between groundwater and phreatophytes

	S1	S2	S3	S4	S5	S6	S7	S8	S9
Soil type[a]	C	C	C	C	C	CL	C	C	C
Root distribution[b]	RP	P	U	RP	RP	RP	RP	RP	RP
LAI (m^2 m^{-2})	1.5	1.5	1.5	3	1.5	1.5	1.5	1.5	1.5
g_{res} (mol m^{-2} s^{-1})	0.04	0.04	0.04	0.04	0.01	0.04	0.04	0.04	0.04
c_a (ppm)	400	400	400	400	400	400	500	400	500
T_a (^{o}C)	-	-	-	-	-	-	-	+1.5	+1.5

[a] Two soil types: clay (C) and clay loam (CL).

[b] Three vertical root distributions: uniform (U), power-law (P) and reverse power-law (RP) rooting profiles. Note that the power-law distribution provides a more realistic description for coniferous species (Andersson, 2005; Finér et al., 1997; Jackson et al., 1996) and a reverse power-law distribution represents plants with only sinker roots extending into groundwater.

List of Figures

1. Schematic of the modeling approach describing the water movement through each compartment of the dynamic groundwater–soil–plant–atmosphere continuum with a summary of the porous medium flow equations, groundwater dynamics and plant hydraulic equations.

2. Cumulative fraction of root length density as a function of depth below soil surface. The total root length density across the rooting depth is 1×10^7 m m^{-3} identical for all scenarios. The two black-dotted lines represent the upper and lower values of predicted daily averaged groundwater level (y) achieved after equilibrium across all scenarios. Note that the power-law distribution provides a more realistic description for coniferous species (Andersson, 2005; Finér et al., 1997; Jackson et al., 1996) and a reverse power-law distribution represents plants with only sinker roots extending into groundwater.

3. Modeled profiles of (a) soil water content (θ_s) and (b) root water influx (q_r^+) or efflux (q_r^-) within a soil layer on a per unit ground area basis for S1 (see Table 2 for model set-up). The black solid line in (a) represents the modeled groundwater level. The first contour line from top in (b) represents zero flux.

4. Modeled time series of (a) groundwater level (y), (b) root water uptake from groundwater ($Q_{r,s}$), (c) transpiration (F_e), and (d) the corresponding recharge rate (O_{in}) from external water body for S1 (see Table 2 for model set-up).

5. Modeled daily averaged (a) stomatal conductance (g_{s,CO_2}), (b) transpiration rate (f_e) and (c) assmilation rate (f_c) after daily equilibrium state for all scenarios.

6. (a) Fraction of root water uptake from the saturated zone ($Q_{r,s}/Q_r$) as a function of root fraction submerged in the saturated zone (R), (b) daily total root water uptake from the saturated zone across all scenarios, and (c) ratio between nighttime and daily total root water uptake from the saturated zone.

7. Comparisons of daily averaged hydraulic redistribution (HR) after daily equilibrium state for different (a) root distributions (reverse power law, power law, and uniform), (b) leaf attributes (increased leaf area index and decreased residual conductance), (c) soil types (clay, and clay loam), and (d) atmospheric conditions (increased atmospheric CO_2 concentration, increased temperature, and increased atmospheric CO_2 concentration and temperature) (see Table 2 for model set-up).

8. Modeled daily averaged groundwater level (y) for different (a) root distributions, (b) leaf attributes, (c) soil types, and (d) atmospheric conditions. Since the predicted daily averaged y's for S1 and S3 in (a) overlap, how they vary at 30-minutes interval is shown in the inset.

9. Modeled nighttime rise of y after daily equilibrium state across all scenarios.

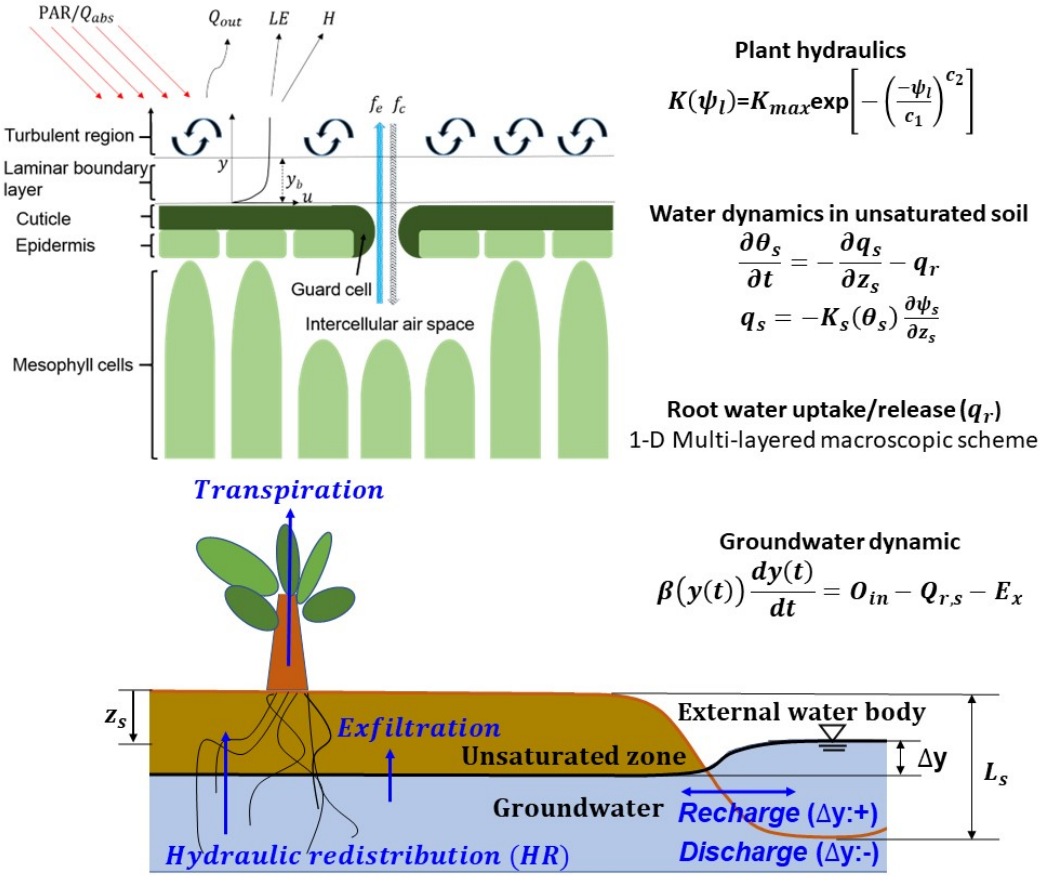

Figure 1: Schematic of the modeling approach describing the water movement through each compartment of the dynamic groundwater–soil–plant–atmosphere continuum with a summary of the porous medium flow equations, groundwater dynamics and plant hydraulic equations.

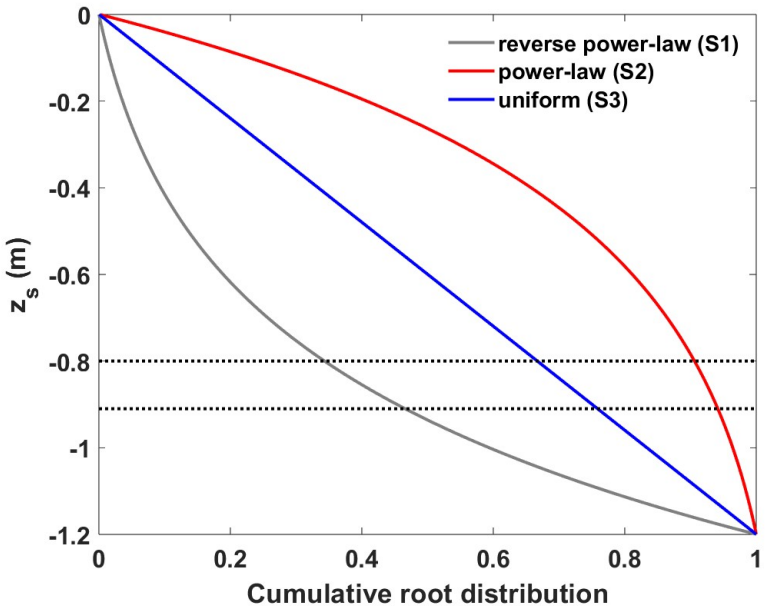

Figure 2: Cumulative fraction of root length density as a function of depth below soil surface. The total root length density across the rooting depth is 1×10^7 m m^{-3} identical for all scenarios. The two black-dotted lines represent the upper and lower values of predicted daily averaged groundwater level (y) after equilibrium state across all scenarios. Note that the power-law distribution provides a more realistic description for coniferous species (Andersson, 2005; Finér et al., 1997; Jackson et al., 1996) and a reverse power-law distribution represents plants with only sinker roots extending into groundwater.

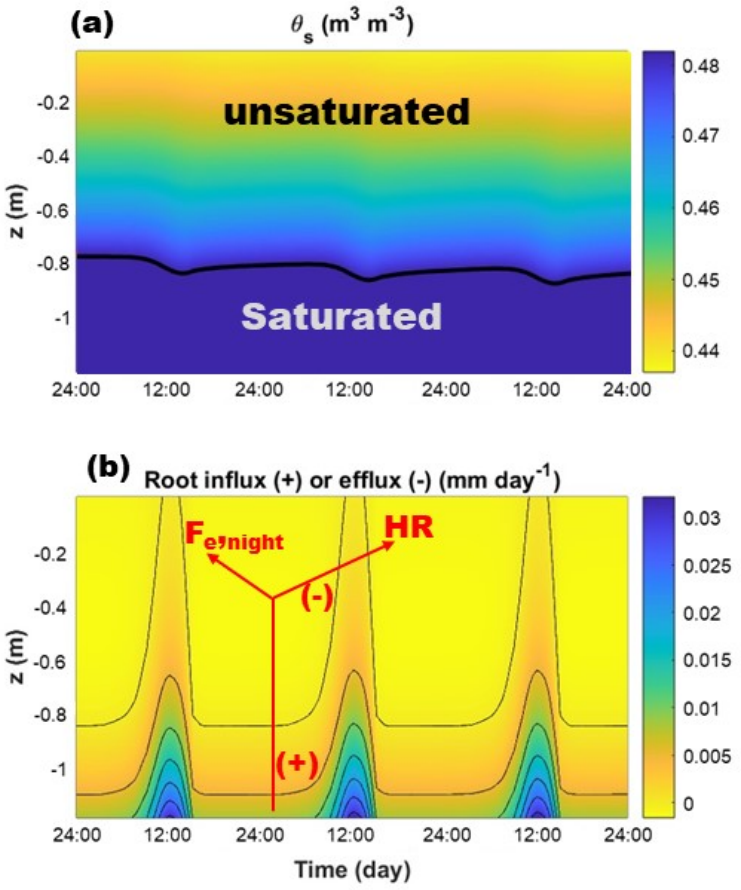

Figure 3: Modeled profiles of (a) soil water content (θ_s) and (b) root water influx (q_r^+) or efflux (q_r^-) within a soil layer on a per unit ground area basis for S1 (see Table 2 for model set-up). The black solid line in (a) represents the modeled groundwater level. The first contour line from top in (b) represents zero flux.

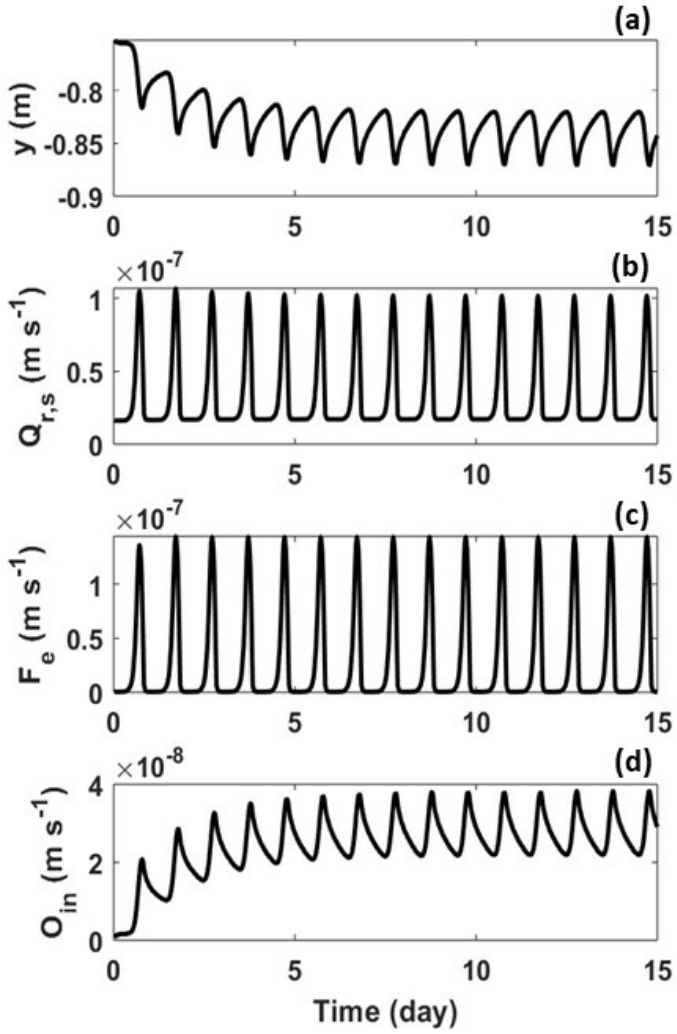

Figure 4: Modeled time series of (a) groundwater level (y), (b) root water uptake from groundwater ($Q_{r,s}$), (c) transpiration (F_e), and (d) the corresponding recharge rate (O_{in}) from external water body for S1 (see Table 2 for model set-up)

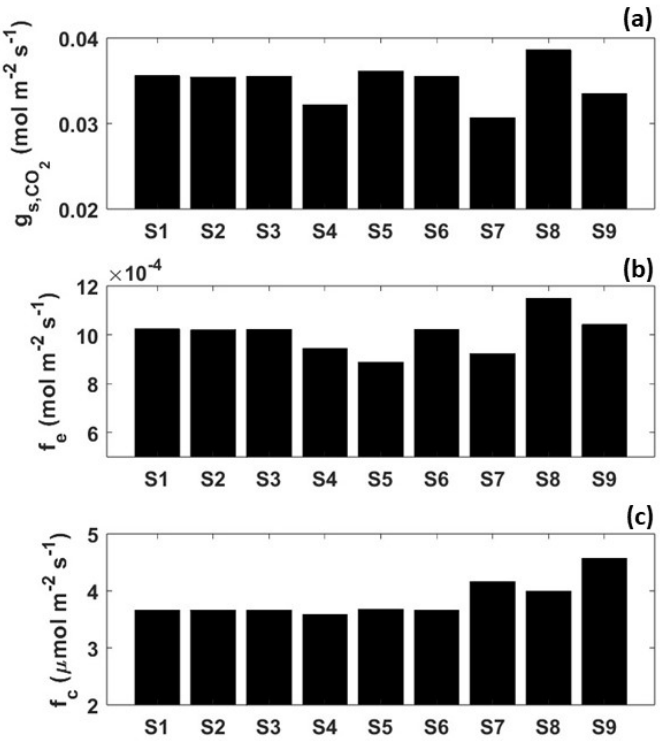

Figure 5: Modeled daily averaged (a) stomatal conductance (g_{s,CO_2}), (b) transpiration rate (f_e) and (c) assmilation rate (f_c) after daily equilibrium state for all scenarios.

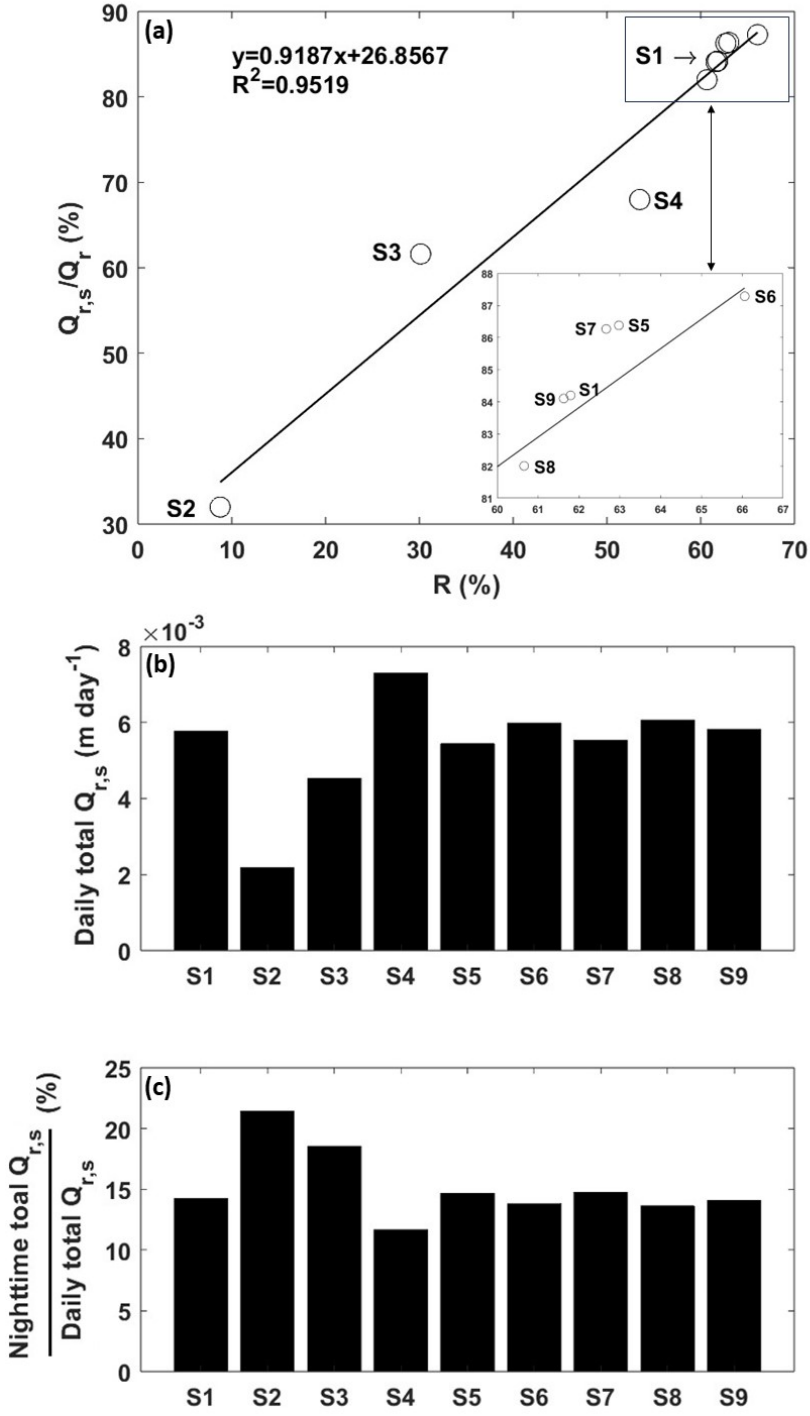

Figure 6: (a) Fraction of root water uptake from the saturated zone ($Q_{r,s}/Q_r$) as a function of root fraction submerged in the saturated zone (R), (b) daily total root water uptake from the saturated zone across all scenarios, and (c) ratio between nighttime and daily total root water uptake from the saturated zone.

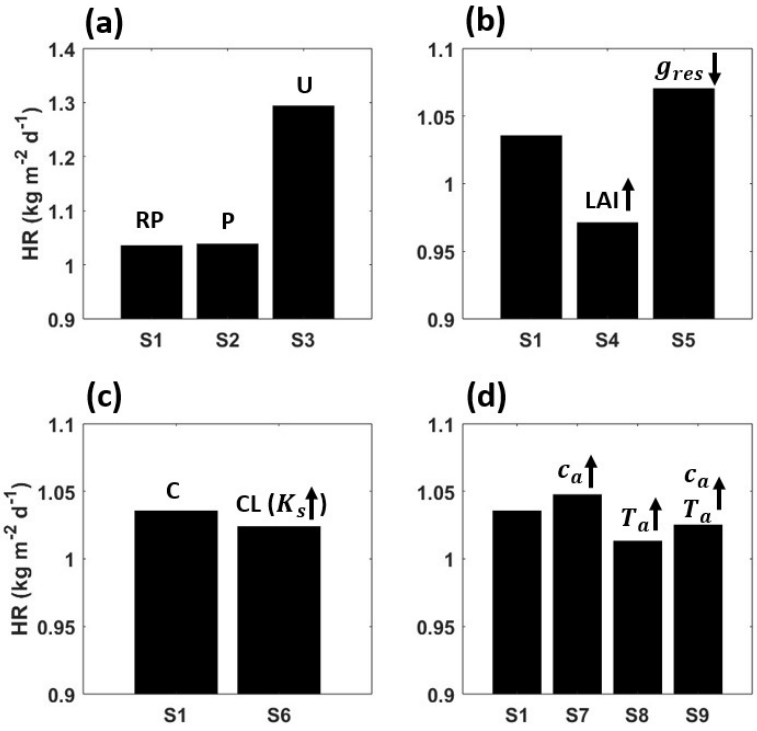

Figure 7: Comparisons of daily averaged hydraulic redistribution (HR) after daily equilibrium state for different (a) root distributions (reverse power law, power law, and uniform), (b) leaf attributes (increased leaf area index and decreased residual conductance), (c) soil types (clay, and clay loam), and (d) atmospheric conditions (increased atmospheric CO_2 concentration, increased temperature, and increased atmospheric CO_2 concentration and temperature) (see Table 2 for model set-up).

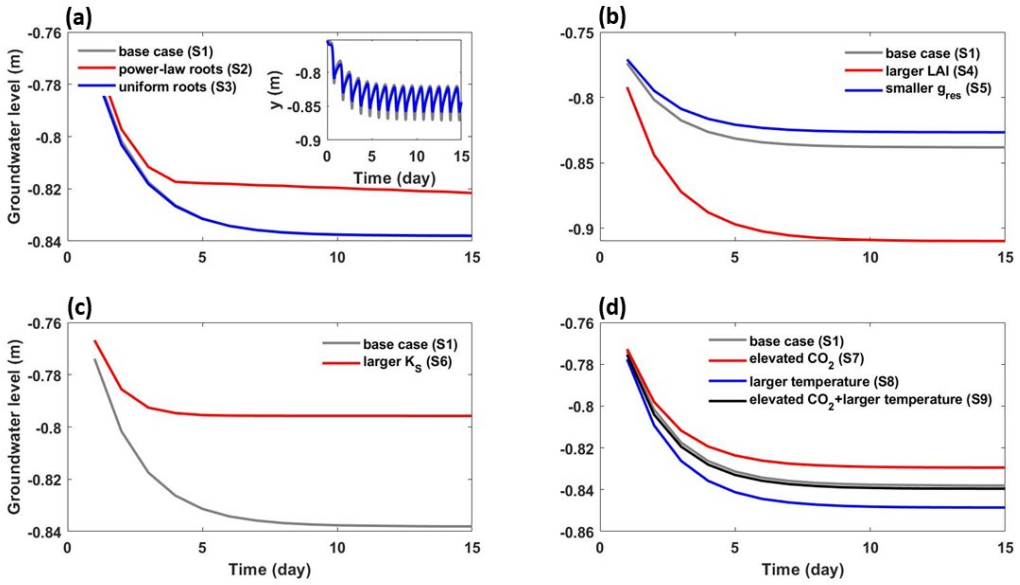

Figure 8: Modeled daily averaged groundwater level (y) for different (a) root distributions, (b) leaf attributes, (c) soil types, and (d) atmospheric conditions. Since the predicted daily averaged y's for S1 and S3 in (a) overlap, how they vary at 30-minutes interval is shown in the inset.

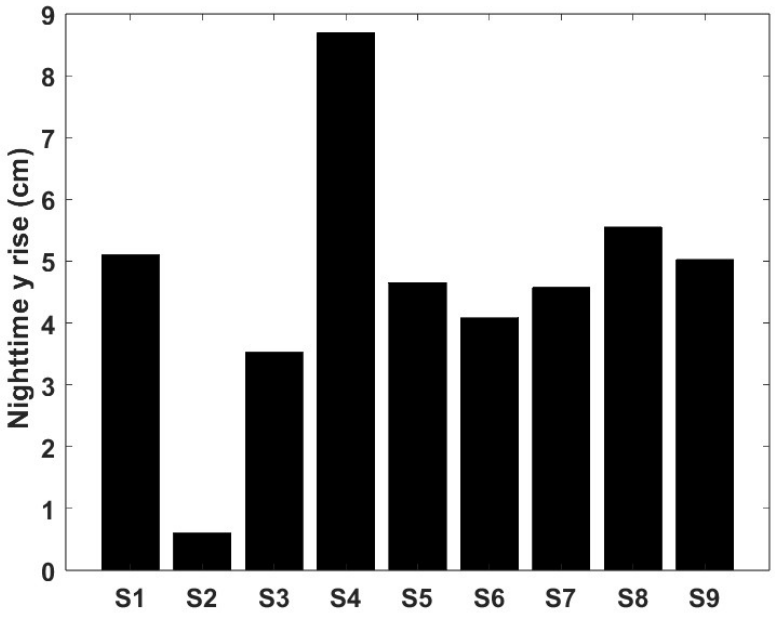

Figure 9: Modeled nighttime rise of y after daily equilibrium state across all scenarios.

A Model parameterization

Model parameters used for the nine scenarios are summarized here. The plant parameters were collected from the literature with a focus on *Pinus taeda* L. When parameters specific for *Pinus taeda* L. were not available, parameters for coniferous species in general and pine plantation trees were adopted. The physiological parameters required for the leaf-level gas exchange and water balance are summarized in Table A.1. The maximum carboxylation capacity ($V_{cmax,25}$) and the light saturated rate of electron transport ($J_{max,25}$) at 25°C are set to be 57 and 98 μmol m^{-2} s^{-1}, respectively (Wullschleger, 1993; Wang et al., 1996; Medlyn et al., 2002). Those physiological values are close to values reported for Loblolly pine at the Duke FACE site (Juang et al., 2008). To explore how nocturnal transpiration impacts groundwater level, g_{res} = 0.01 and 0.04 mol m^{-2} s^{-1} are assumed to reflect small and large nocturnal transpiration conditions. The choice of g_{res} resides in the range for numerous coniferous species as summarized elsewhere (Caird et al., 2007). The empirical parameters of the λ-$\overline{\psi}_l$ relation (i.e., λ^* and α) are taken for the coniferous species reported elsewhere (Manzoni et al., 2011). The model parameters for the xylem vulnerability curve are taken to be within the range for pine from the literature (Cochard, 1992; Domec and Gartner, 2001; Manzoni et al., 2013a; Phillips et al., 2004), and are listed in Table A.2. The root properties and soil hydraulic parameters are provided in Table A.3 and A.4, respectively. The rooting profiles are chosen to be uniformly distributed or varied using a power-law reduction (Jackson et al., 1996) or reverse power-law function, given that the total root density within the rooting depth (L_R) is held constant. Two different soil types – clay and clay loam (Clapp and Hornberger, 1978) – are used to explore the model behavior for different soil texture. Fig.A.1 shows the diurnal variation of the atmospheric variables used to drive the model simulations. This 24-h time series of the atmospheric variables was determined by ensemble averaging across summer periods by time of day and represents the typical summertime meteorological variables at the Blackwood Division of the Duke Forest (35.971^{o}N, 79.09^{o}W, elevation 163 m) near Durham, North Carolina (Volpe et al., 2013).

Table A.1: Leaf-level physiological attributes

Parameters	Value	Unit
$V_{cmax,25}$	57	μmol m^{-2} s^{-1}
$J_{max,25}$	98	μmol m^{-2} s^{-1}
g_{res}	0.01 or 0.04	mol m^{-2} s^{-1}
λ^{*a}	6.55	μmol mol^{-1} kPa^{-1}
α^{a}	1.56	MPa^{-1}

[a] The parameters of relation were adopted for conifers in arid or semiarid climates (Manzoni et al., 2011).

Table A.2: Xylem hydraulic parameters

Parameters	Value	Unit
K_{max}	1.5×10^{-6}	kg s^{-1} MPa^{-1}
c_1	4.8	MPa
c_2	3.5	Dimensionless

Table A.3: Root properties

Parameters	Value	Unit
L_R	1.2	m
k_r	10^{-9}	s^{-1}
	Formulation	Unit
B_U	6354	m m^{-3}
B_P[a]	$19586 \times 0.976^{100 z_s}$	m m^{-3}
B_{RP}	$19586 \times 0.976^{100(L_R - z_s)}$	m m^{-3}

[a] The power law reduction function describing the vertical root length distribution is adopted from elsewhere (Jackson et al., 1996) for conifers. Note that the total root density across L_R is identical for all scenarios.

Table A.4: Soil properties

Parameters	Value	Unit
Clay[a]		
$K_{s,max}$	1.3×10^{-6}	m s^{-1}
$\theta_{s,sat}$	0.482	m^3 m^{-3}
$\phi_{s,sat}$	-0.405	m
b	11.4	Dimensionless
Clay loam[a]		
$K_{s,max}$	2.5×10^{-6}	m s^{-1}
$\theta_{s,sat}$	0.476	m^3 m^{-3}
$\phi_{s,sat}$	-0.63	m
b	8.52	Dimensionless

[a] The hydraulic parameters for the two soil types are taken from elsewhere (Clapp and Hornberger, 1978).

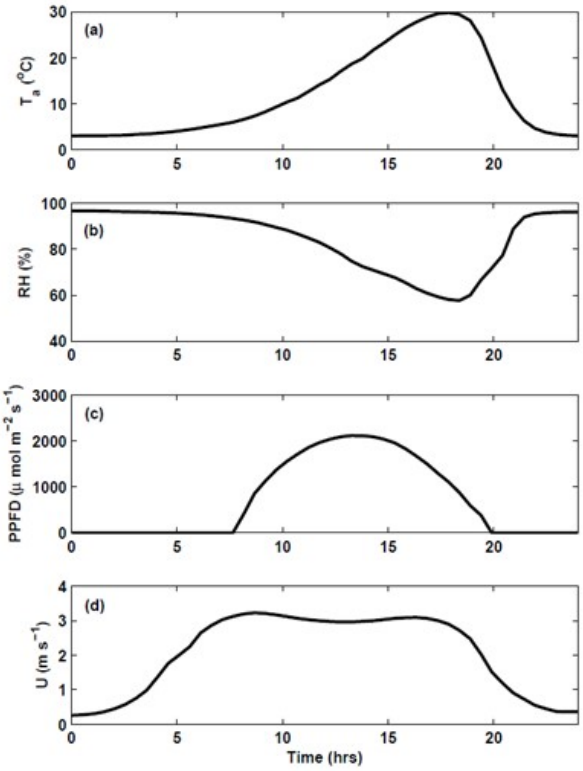

Figure A.1: The diurnal variations of (a) air temperature (T_a), (b) relative humidity (RH), (c) photosynthetically active radiation ($PPFD$), and (d) wind speed (U).

References

Aguilos, M., Sun, G., Noormets, A., Domec, J.C., McNulty, S., Gavazzi, M., Prajapati, P., Minick, K.J., Mitra, B., King, J., 2021. Ecosystem productivity and evapotranspiration are tightly coupled in loblolly pine (pinus taeda l.) plantations along the coastal plain of the southeastern us. Forests 12, 1123.

Ahmed, I., Umar, R., 2009. Groundwater flow modelling of yamuna-krishni interstream, a part of central ganga plain uttar pradesh. Journal of Earth System Science 118, 507–523.

Andersson, F., 2005. Coniferous forests. volume 6. Elsevier.

Aphalo, P., Jarvis, P., 1991. Do stomata respond to relative humidity? Plant, Cell and Environment 14, 127–132.

Bear, J., 1988. Dynamics of fluids in porous media. Courier Corporation.

Bonetti, S., Manoli, G., Domec, J.C., Putti, M., Marani, M., Katul, G., 2015. The influence of water table depth and the free atmospheric state on convective rainfall predisposition. Water Resources Research 51, 2283–2297.

Boyer, J.S., Wong, S.C., Farquhar, G.D., 1997. CO2 and water vapor exchange across leaf cuticle (epidermis) at various water potentials. Plant Physiology 114, 185–191.

Brooks, J.R., Meinzer, F.C., Warren, J.M., DOMEC, J.C., Coulombe, R., 2006. Hydraulic redistribution in a douglas-fir forest: lessons from system manipulations. Plant, Cell & Environment 29, 138–150.

Burgess, S.S., Pate, J.S., Adams, M.A., Dawson, T.E., 2000. Seasonal water acquisition and redistribution in the australian woody phreatophyte, *Banksia prionotes*. Annals of Botany 85, 215–224.

Butler Jr, J.J., Kluitenberg, G.J., Whittemore, D.O., Loheide, S.P., Jin, W., Billinger, M.A., Zhan, X., 2007. A field investigation of phreatophyte-induced fluctuations in the water table. Water Resources Research 43.

Caird, M.A., Richards, J.H., Donovan, L.A., 2007. Nighttime stomatal conductance and transpiration in C_3 and C_4 plants. Plant Physiology 143, 4–10.

Campbell, G.S., Norman, J., 1998. An introduction to environmental biophysics. Springer, New York.

Canham, C.A., Froend, R.H., Stock, W.D., Davies, M., 2012. Dynamics of phreatophyte root growth relative to a seasonally fluctuating water table in a mediterranean-type environment. Oecologia 170, 909–916.

Carlson Mazur, M.L., Wiley, M.J., Wilcox, D.A., 2014a. Estimating evapotranspiration and groundwater flow from water-table fluctuations for a general wetland scenario. Ecohydrology 7, 378–390.

Carlson Mazur, M.L., Wiley, M.J., Wilcox, D.A., 2014b. Estimating evapotranspiration and groundwater flow from water-table fluctuations for a general wetland scenario. Ecohydrology 7, 378–390.

Cernusak, L.A., Goldsmith, G.R., Arend, M., Siegwolf, R.T., 2019. Effect of vapor pressure deficit on gas exchange in wild-type and abscisic acid–insensitive plants. Plant Physiology 181, 1573–1586.

Cernusak, L.A., Ubierna, N., Jenkins, M.W., Garrity, S.R., Rahn, T., Powers, H.H., Hanson, D.T., Sevanto, S., Wong, S.C., McDowell, N.G., et al., 2018. Unsaturation of vapour pressure inside leaves of two conifer species. Scientific reports 8, 7667.

Clapp, R., Hornberger, G., 1978. Empirical equations for some soil hydraulic properties. Water Resources Research 14, 601–604.

Cochard, H., 1992. Vulnerability of several conifers to air embolism. Tree physiology 11, 73–83.

Cooper, D.J., Sanderson, J.S., Stannard, D.I., Groeneveld, D.P., 2006. Effects of long-term water table drawdown on evapotranspiration and vegetation in an arid region phreatophyte community. Journal of Hydrology 325, 21–34.

Cowan, I., Farquhar, G., 1977. Stomatal function in relation to leaf metabolism and environment. In: Integration of activity in the higher plant. Symposia of the Society for Experimental Biology. volume 31. Cambridge University Press, Cambridge.

Crosbie, R.S., Doble, R.C., Turnadge, C., Taylor, A.R., 2019. Constraining the magnitude and uncertainty of specific yield for use in the water table fluctuation method of estimating recharge. Water Resources Research 55, 7343–7361.

Dawson, T.E., Burgess, S.S.O., Tu, K.P., Oliveira, R.S., Santiago, L.S., Fisher, J.B., Simonin, K.A., Ambrose, A.R., 2007. Nighttime transpiration in woody plants from contrasting ecosystems. Tree Physiology 27, 561–575.

Döll, P., Hoffmann-Dobrev, H., Portmann, F.T., Siebert, S., Eicker, A., Rodell, M., Strassberg, G., Scanlon, B., 2012. Impact of water withdrawals from groundwater and surface water on continental water storage variations. Journal of Geodynamics 59, 143–156.

Domec, J., Gartner, B., 2001. Cavitation and water storage capacity in bole xylem segments of mature and young Douglas-fir trees. Trees 15, 204–214.

Domec, J., King, J.S., Noormets, A., Treasure, E., Gavazzi, M., Sun, G., McNulty, S., 2010. Hydraulic redistribution of soil water by roots affects whole-stand evapotranspiration and net ecosystem carbon exchange. New Phytologist 187, 171–183.

Domec, J.C., Ogée, J., Noormets, A., Jouangy, J., Gavazzi, M., Treasure, E., Sun, G., McNulty, S.G., King, J.S., 2012a. Interactive effects of nocturnal transpiration and climate change on the root hydraulic redistribution and carbon and water budgets of southern United States pine plantations. Tree Physiology 32, 707–723.

Domec, J.C., Sun, G., Noormets, A., Gavazzi, M.J., Treasure, E.A., Cohen, E., Swenson, J.J., McNulty, S.G., King, J.S., 2012b. A comparison of three methods to estimate evapotranspiration in two contrasting loblolly pine plantations: age-related changes in water use and drought sensitivity of evapotranspiration components. Forest Science 58, 497–512.

Domec, J.C., Warren, J., Meinzer, F., Brooks, J., Coulombe, R., 2004. Native root xylem embolism and stomatal closure in stands of douglas-fir and ponderosa pine: mitigation by hydraulic redistribution. Oecologia 141, 7–16.

Dusenge, M.E., Duarte, A.G., Way, D.A., 2019. Plant carbon metabolism and climate change: elevated co 2 and temperature impacts on photosynthesis, photorespiration and respiration. New Phytologist 221, 32–49.

Eamus, D., Froend, R., Loomes, R., Hose, G., Murray, B., 2006. A functional methodology for determining the groundwater regime needed to maintain the health of groundwater-dependent vegetation. Australian Journal of Botany 54, 97–114.

Fahle, M., Dietrich, O., 2014. Estimation of evapotranspiration using diurnal groundwater level fluctuations: Comparison of different approaches with groundwater lysimeter data. Water Resources Research 50, 273–286.

Farquhar, G.D., von Caemmerer, S., Berry, J.A., 1980. A biochemical model of photosynthetic CO_2 assimilation in leaves of C_3 species. Planta 149, 78–90.

Feddes, R.A., Kowalik, P., Kolinska-Malinka, K., Zaradny, H., 1976. Simulation of field water uptake by plants using a soil water dependent root extraction function. Journal of Hydrology 31, 13–26.

Finér, L., Messier, C., De Grandpré, L., 1997. Fine-root dynamics in mixed boreal conifer-broad-leafed forest stands at different successional stages after fire. Canadian Journal of Forest Research 27, 304–314.

Garcia, C.A., Huntington, J.M., Buto, S.G., Moreo, M.T., Smith, J., Andraski, B.J., 2015. Groundwater Discharge by Evapotranspiration, Dixie Valley, West-central Nevada, March 2009-September 2011. US Department of the Interior, US Geological Survey.

García Suárez, F., Fulginiti, L.E., Perrin, R.K., 2019. What is the use value of irrigation water from the high plains aquifer? American Journal of Agricultural Economics 101, 455–466.

Gardner, W., 1958. Some steady-state solutions of the unsaturated moisture flow equation with application to evaporation from a water table. Soil science 85, 228–232.

Givnish, T.J., Vermeij, G.J., 1976. Sizes and shapes of liane leaves. American Naturalist 110, 743–778.

Gleeson, T., Cuthbert, M., Ferguson, G., Perrone, D., 2020. Global groundwater sustainability, resources, and systems in the anthropocene. Annual review of earth and planetary sciences 48, 431–463.

Gou, S., Miller, G., 2014. A groundwater–soil–plant–atmosphere continuum approach for modelling water stress, uptake, and hydraulic redistribution in phreatophytic vegetation. Ecohydrology 7, 1029–1041.

Gou, S., Miller, G.R., Saville, C., Maxwell, R.M., Ferguson, I.M., 2018. Simulating groundwater uptake and hydraulic redistribution by phreatophytes in a high-resolution, coupled subsurface-land surface model. Advances in Water Resources 121, 245–262.

Grantz, D., 1990. Plant response to atmospheric humidity. Plant, Cell and Environment 13, 667–679.

Gribovszki, Z., 2018. Comparison of specific-yield estimates for calculating evapotranspiration from diurnal groundwater-level fluctuations. Hydrogeology Journal 26, 869–880.

Gribovszki, Z., Kalicz, P., Szilágyi, J., Kucsara, M., 2008. Riparian zone evapotranspiration estimation from diurnal groundwater level fluctuations. Journal of Hydrology 349, 6–17.

Grimaldi, S., Orellana, F., Daly, E., 2015. Modelling the effects of soil type and root distribution on shallow groundwater resources. Hydrological Processes 29, 4457–4469.

Healy, R.W., Cook, P.G., 2002. Using groundwater levels to estimate recharge. Hydrogeology journal 10, 91–109.

Hernandez, J.O., 2022. Ecophysiological effects of groundwater drawdown on phreatophytes: Research trends during the last three decades. Land 11, 2061.

Howard, A.R., Van Iersel, M.W., Richards, J.H., Donovan, L.A., 2009. Night-time transpiration can decrease hydraulic redistribution. Plant, Cell and Environment 32, 1060–1070.

Hsieh, P.A., Wingle, W., Healy, R.W., 2000. VS2DI-A graphical software package for simulating fluid flow and solute or energy transport in variably saturated porous media. Technical Report. US Geological Survey.

Huang, C.W., Chu, C.R., Hsieh, C.I., Palmroth, S., Katul, G.G., 2015. Wind-induced leaf transpiration. Advances in Water Resources 86, 240–255. doi:doi:10.1016/j.advwatres.2015.10.009.

Huang, C.W., Domec, J.C., Palmroth, S., Pockman, W.T., Litvak, M.E., Katul, G.G., 2018. Transport in a coordinated soil-root-xylem-phloem leaf system. Advances in Water Resources 119, 1–16.

Huang, C.W., Domec, J.C., Ward, E.J., Duman, T., Manoli, G., Parolari, A.J., Katul, G.G., 2017. The effect of plant water storage on water fluxes within the coupled soil–plant system. New Phytologist 213, 1093–1106. URL: http://dx.doi.org/10.1111/nph.14273, doi:10.1111/nph.14273.

Hultine, K., Williams, D., Burgess, S., Keefer, T., 2003. Contrasting patterns of hydraulic redistribution in three desert phreatophytes. Oecologia 135, 167–175.

IPCC, 2013. Climate change 2013: the physical science basis. *In: Stocker, T. F. and Qin, D. and Plattner, G. K. and Tignor, M. and Allen, S. K. and Boschung, J. and Nauels, A. and Xia, Y. and Bex, B. and Midgley, B. M. (Eds),* Working Group I contribution to the Fifth assessment report of the Intergovernmental Panel on Climate Change. Cambridge University Press.

Jackson, R., Canadell, J., Ehleringer, J., Mooney, H., Sala, O., Schulze, E., 1996. A global analysis of root distributions for terrestrial biomes. Oecologia 108, 389–411.

Jarrell, W., Virginia, R., 1990. Response of mesquite to nitrate and salinity in a simulated phreatic environment: water use, dry matter and mineral nutrient accumulation. Plant and Soil 125, 185–196.

Jiang, X.W., Sun, Z.C., Zhao, K.Y., Shi, F.S., Wan, L., Wang, X.S., Shi, Z.M., 2017. A method for simultaneous estimation of groundwater evapotranspiration and inflow rates in the discharge area using seasonal water table fluctuations. Journal of hydrology 548, 498–507.

Juang, J., Katul, G.G., Siqueira, M., Stoy, P., McCarthy, H., 2008. Investigating a hierarchy of eulerian closure models for scalar transfer inside forested canopies. Boundary-Layer Meteorology 128, 1–32.

Katul, G.G., Oren, R., Manzoni, S., Higgins, C., Parlange, M.B., 2012. Evapotranspiration: A process driving mass transport and energy exchange in the soil-plant-atmosphere-climate system. Reviews of Geophysics 50, RG3002. doi:10.1029/2011RG000366.

Katul, G.G., Palmroth, S., Oren, R., 2009. Leaf stomatal responses to vapour pressure deficit under current and CO_2-enriched atmosphere explained by the economics of gas exchange. Plant, cell and environment 32, 968–979.

Kavanagh, K., Bond, B., Aitken, S., Gartner, B., Knowe, S., 1999. Shoot and root vulnerability to xylem cavitation in four populations of Douglas-fir seedlings. Tree Physiology 19, 31–37.

Kirschbaum, M.U., McMillan, A.M., 2018. Warming and elevated co 2 have opposing influences on transpiration. which is more important? Current Forestry Reports 4, 51–71.

Koirala, S., Jung, M., Reichstein, M., de Graaf, I.E., Camps-Valls, G., Ichii, K., Papale, D., Ráduly, B., Schwalm, C.R., Tramontana, G., et al., 2017. Global distribution of groundwater-vegetation spatial covariation. Geophysical Research Letters 44, 4134–4142.

Kollet, S.J., Maxwell, R.M., 2006. Integrated surface–groundwater flow modeling: A free-surface overland flow boundary condition in a parallel groundwater flow model. Advances in Water Resources 29, 945–958.

Kollet, S.J., Maxwell, R.M., 2008. Capturing the influence of groundwater dynamics on land surface processes using an integrated, distributed watershed model. Water Resources Research 44.

Konrad, W., Roth-Nebelsick, A., Grein, M., 2008. Modelling of stomatal density response to atmospheric CO_2. Journal of Theoretical Biology 253, 638–658.

Laczniak, R.J., DeMeo, G.A., Reiner, S.R., Smith, J., Nylund, W.E., 1999. Estimates of groundwater discharge as determined from measurements of evapotranspiration, Ash Meadows Area, Nye County, Nevada. Technical Report. Geological Survey, Las Vegas, NV (US).

Lafolie, F., Bruckler, L., Tardieu, F., 1991. Modeling root water potential and soil-root water transport: I. Model presentation. Soil Science Society of America Journal 55, 1203–1212.

Laio, F., Tamea, S., Ridolfi, L., D'Odorico, P., Rodriguez-Iturbe, I., 2009. Ecohydrology of groundwater-dependent ecosystems: 1. stochastic water table dynamics. Water Resources Research 45.

Larcher, W., 2003. Physiological plant ecology: ecophysiology and stress physiology of functional groups. Springer Science & Business Media.

Lautz, L.K., 2008. Estimating groundwater evapotranspiration rates using diurnal water-table fluctuations in a semi-arid riparian zone. Hydrogeology Journal 16, 483–497.

Lendzion, J., Leuschner, C., 2008. Growth of european beech (*Fagus sylvatica* L.) saplings is limited by elevated atmospheric vapour pressure deficits. Forest Ecology and Management 256, 648–655.

Loheide, S.P., Butler Jr, J.J., Gorelick, S.M., 2005. Estimation of groundwater consumption by phreatophytes using diurnal water table fluctuations: A saturated-unsaturated flow assessment. Water resources research 41.

Lu, N., Likos, W., 2004. Rate of capillary rise in soil. Journal of geotechnical and Geoenvironmental engineering 130, 646–650.

Manoli, G., Bonetti, S., Domec, J.C., Putti, M., Katul, G., Marani, M., 2014. Tree root systems competing for soil moisture in a 3D soil-plant model. Advances in Water Resources 66, 32–42.

Mansfield, T., Hetherington, A., Atkinson, C., 1990. Some current aspects of stomatal physiology. Annual review of plant biology 41, 55–75.

Manzoni, S., Katul, G., Porporato, A., 2014. A dynamical system perspective on plant hydraulic failure. Water Resources Research 50, 5170–5183.

Manzoni, S., Vico, G., Katul, G., Fay, P.A., Polley, W., Palmroth, S., Porporato, A., 2011. Optimizing stomatal conductance for maximum carbon gain under water stress: a meta-analysis across plant functional types and climates. Functional Ecology 25, 456–467.

Manzoni, S., Vico, G., Katul, G., Palmroth, S., Jackson, R.B., Porporato, A., 2013a. Hydraulic limits on maximum plant transpiration and the emergence of the safety-efficiency trade-off. New Phytologist 198, 169–178.

Manzoni, S., Vico, G., Palmroth, S., Porporato, A., Katul, G., 2013b. Optimization of stomatal conductance for maximum carbon gain under dynamic soil moisture. Advances in Water Resources 62, 90–105.

Manzoni, S., Vico, G., Porporato, A., Katul, G., 2013c. Biological constraints on water transport in the soil-plant-atmosphere system. Advances in Water Resources 51, 292–304.

Massman, W., Kaufmann, M., 1991. Stomatal response to certain environmental factors: a comparison of models for subalpine trees in the Rocky Mountains. Agricultural and Forest Meteorology 54, 155–167.

Maxwell, R.M., Miller, N.L., 2005. Development of a coupled land surface and groundwater model. Journal of Hydrometeorology 6, 233–247.

McAdam, S.A., Brodribb, T.J., 2015. The evolution of mechanisms driving the stomatal response to vapor pressure deficit. Plant Physiology 167, 833–843.

McGuire, V.L., 2017. Water-level and recoverable water in storage changes, high plains aquifer, predevelopment to 2015 and 2013–15 .

Medlyn, B.E., Dreyer, E., Ellsworth, D., Forstreuter, M., Harley, P.C., Kirschbaum, M.U.F., Le Roux, X., Montpied, P., Strassemeyer, J., Walcroft, A., 2002. Temperature response of parameters of a biochemically based model of photosynthesis. II. a review of experimental data. Plant, Cell and Environment 25, 1167–1179.

Messinger, S.M., Buckley, T.N., Mott, K.A., 2006. Evidence for involvement of photosynthetic processes in the stomatal response to CO_2. Plant Physiology 140, 771–778.

Monteith, J., 1995. A reinterpretation of stomatal responses to humidity. Plant, Cell and Environment 18, 357–364.

Mooney, H.A., Gulmon, S., Rundel, P.W., Ehleringer, J., 1980. Further observations on the water relations ofprosopis tamarugo of the northern atacama desert. Oecologia 44, 177–180.

Moreo, M.T., Andraski, B.J., Garcia, C.A., 2017. Groundwater discharge by evapotranspiration, flow of water in unsaturated soil, and stable isotope water sourcing in areas of sparse vegetation, Amargosa Desert, Nye County, Nevada. Technical Report. US Geological Survey.

Morison, J.I., 1998. Stomatal response to increased CO_2 concentration. Journal of Experimental Botany 49, 443–452.

Morison, J.I., Gifford, R.M., 1983. Stomatal sensitivity to carbon dioxide and humidity. A comparison of two C3 and two C4 grass species. Plant physiology 71, 789–796.

Morris, B.L., Lawrence, A.R., Chilton, P., Adams, B., Calow, R.C., Klinck, B.A., 2003. Groundwater and its susceptibility to degradation: a global assessment of the problem and options for management. United Nations Environment Programme.

Mott, K.A., 1988. Do stomata respond to CO_2 concentrations other than intercellular? Plant Physiology 86, 200–203.

Nachabe, M.H., 2002. Analytical expressions for transient specific yield and shallow water table drainage. Water resources research 38, 11–1.

Naumburg, E., Mata-Gonzalez, R., Hunter, R.G., Mclendon, T., Martin, D.W., 2005. Phreatophytic vegetation and groundwater fluctuations: a review of current research and application of ecosystem response modeling with an emphasis on great basin vegetation. Environmental Management 35, 726–740.

Neumann, R., Cardon, Z., 2012. The magnitude of hydraulic redistribution by plant roots: a review and synthesis of empirical and modeling studies. New Phytologist 194, 337–352.

Nichols, W.D., 1993. Estimating discharge of shallow groundwater by transpiration from greasewood in the northern great basin. Water Resources Research 29, 2771–2778.

Nichols, W.D., 1994. Groundwater discharge by phreatophyte shrubs in the great basin as related to depth to groundwater. Water Resources Research 30, 3265–3274.

Novick, K.A., Oren, R., Stoy, P.C., Siqueira, M.B.S., Katul, G.G., 2009. Nocturnal evapotranspiration in eddy covariance records from three colocated ecosystems in the Southeastern U.S.: Implications for annual fluxes. Agricultural and Forest Meteorology 149, 1491–1504.

Orellana, F., Verma, P., Loheide, S.P., Daly, E., 2012. Monitoring and modeling water-vegetation interactions in groundwater-dependent ecosystems. Reviews of Geophysics 50.

Oren, R., Sperry, J.S., Katul, G., Pataki, D.E., Ewers, B., Phillips, N., Schäfer, K., 1999. Survey and synthesis of intra- and interspecific variation in stomatal sensitivity to vapour pressure deficit. Plant, Cell and Environment 22, 1515–1526.

Phillips, N.G., Oren, R., Licata, J., Linder, S., 2004. Time series diagnosis of tree hydraulic characteristics. Tree Physiology 24, 879–890.

Prieto, I., Armas, C., Pugnaire, F., 2012. Water release through plant roots: new insights into its consequences at the plant and ecosystem level. New Phytologist 193, 830–841.

Prieto, I., Kikvidze, Z., Pugnaire, F., 2010. Hydraulic lift: soil processes and transpiration in the mediterranean leguminous shrub *Retama sphaerocarpa* (L.) boiss. Plant and Soil 329, 447–456.

Rateb, A., Scanlon, B.R., Pool, D.R., Sun, A., Zhang, Z., Chen, J., Clark, B., Faunt, C.C., Haugh, C.J., Hill, M., et al., 2020. Comparison of groundwater storage changes from grace satellites with monitoring and modeling of major us aquifers. Water Resources Research 56, e2020WR027556.

Ridolfi, L., D'Odorico, P., Laio, F., Tamea, S., Rodriguez-Iturbe, I., 2008. Coupled stochastic dynamics of water table and soil moisture in bare soil conditions. Water resources research 44.

Rodriguez-Iturbe, I., D'Odorico, P., Laio, F., Ridolfi, L., Tamea, S., 2007. Challenges in humid land ecohydrology: Interactions of water table and unsaturated zone with climate, soil, and vegetation. Water Resources Research 43.

Scanlon, B., Reedy, R., Gates, J., Gowda, P., 2010. Impact of agroecosystems on groundwater resources in the central high plains, usa. Agriculture, ecosystems & environment 139, 700–713.

Scanlon, B.R., Fakhreddine, S., Rateb, A., de Graaf, I., Famiglietti, J., Gleeson, T., Grafton, R.Q., Jobbagy, E., Kebede, S., Kolusu, S.R., et al., 2023. Global water resources and the role of groundwater in a resilient water future. Nature Reviews Earth & Environment 4, 87–101.

Scanlon, B.R., Jolly, I., Sophocleous, M., Zhang, L., 2007. Global impacts of conversions from natural to agricultural ecosystems on water resources: Quantity versus quality. Water resources research 43.

Scholz, F., Bucci, S., Goldstein, G., Moreira, M., Meinzer, F., Domec, J.C., Villalobos-Vega, R., Franco, A., Miralles-Wilhelm, F., 2008. Biophysical and life-history determinants of hydraulic lift in Neotropical savanna trees. Functional Ecology 22, 773–786.

Siebert, S., Burke, J., Faures, J.M., Frenken, K., Hoogeveen, J., Döll, P., Portmann, F.T., 2010. Groundwater use for irrigation–a global inventory. Hydrology and earth system sciences 14, 1863–1880.

Simunek, J., Van Genuchten, M.T., 1999. Manual of hydrus-2d computer program for simulation water flow, heat and solute transport in variably saturated porous media. USDA, Riverside, CA .

Siqueira, M., Katul, G., Porporato, A., 2008. Onset of water stress, hysteresis in plant conductance, and hydraulic lift: scaling soil water dynamics from millimeters to meters. Water Resources Research 44.

Soylu, M.E., Lenters, J.D., Istanbulluoglu, E., Loheide, S.P., 2012. On evapotranspiration and shallow groundwater fluctuations: A fourier-based improvement to the white method. Water Resources Research 48.

Todd, D.K., Mays, L.W., 2004. Groundwater hydrology. John Wiley & Sons.

UNESCO World Water Assessment Programme (WWAP), 2022. The United Nations World Water Development Report 2022: Groundwater – Making the Invisible Visible. UNESCO, Paris. URL: https://www.unesco.org/reports/wwdr/2022.

Vogel, T., Dohnal, M., Dusek, J., Votrubova, J., Tesar, M., 2013. Macroscopic modeling of plant water uptake in a forest stand involving root-mediated soil water redistribution. Vadose Zone Journal 12.

Volpe, V., Marani, M., Albertson, J.D., Katul, G.G., 2013. Root controls on water redistribution and carbon uptake in the soil-plant system under current and future climate. Advances in Water Resources 60, 110–120.

Wahlenberg, W.G., et al., 1960. Loblolly pine. its use, ecology, regeneration, protection, growth and management. Loblolly Pine. Its use, ecology, regeneration, protection, growth and management. .

Wang, K.Y., Kellomaki, S., Laitinen, K., 1996. Acclimation of photosynthetic parameters in Scots pine after three years exposure to elevated temperature and CO_2. Agricultural and Forest Meteorology 82, 195–217. doi:Doi10.1016/0168-1923(96)02329-5.

Wang, P., Grinevsky, S.O., Pozdniakov, S.P., Yu, J., Dautova, D.S., Min, L., Du, C., Zhang, Y., 2014. Application of the water table fluctuation method for estimating evapotranspiration at two phreatophyte-dominated sites under hyper-arid environments. Journal of Hydrology 519, 2289–2300.

Wang, T., Wu, Z., Wang, P., Wu, T., Zhang, Y., Yin, J., Yu, J., Wang, H., Guan, X., Xu, H., et al., 2023. Plant-groundwater interactions in drylands: A review of current research and future perspectives. Agricultural and Forest Meteorology 341, 109636.

Wang, T.Y., Wang, P., Wang, Z.L., Niu, G.Y., Yu, J.J., Ma, N., Wu, Z.N., Pozdniakov, S.P., Yan, D.H., 2021. Drought adaptability of phreatophytes: insight from vertical root distribution in drylands of china. Journal of Plant Ecology 14, 1128–1142.

Wang, X., Tang, C., Guppy, C., Sale, P.W.G., 2009. The role of hydraulic lift and subsoil P placement in P uptake of cotton (*Gossypium hirsutum* L.). Plant and Soil 325, 263–275.

Warren, J.M., Meinzer, F.C., Brooks, J.R., Domec, J.C., Coulombe, R., 2007. Hydraulic redistribution of soil water in two old-growth coniferous forests: Quantifying patterns and controls. New Phytologist 173, 753–765.

White, W.N., 1932. A method of estimating ground-water supplies based on discharge by plants and evaporation from soil: Results of investigations in Escalante Valley, Utah. volume 659. US Government Printing Office.

Wong, S.C., Canny, M.J., Holloway-Phillips, M., Stuart-Williams, H., Cernusak, L.A., Márquez, D.A., Farquhar, G.D., 2022. Humidity gradients in the air spaces of leaves. Nature Plants 8, 971–978.

Wullschleger, S.D., 1993. Biochemical limitations to carbon assimilation in C_3 plants-a retrospective analysis of the A/C_i curves from 109 species. Journal of Experimental Botany 44, 907–920.

Yin, L., Zhou, Y., Ge, S., Wen, D., Zhang, E., Dong, J., 2013. Comparison and modification of methods for estimating evapotranspiration using diurnal groundwater level fluctuations in arid and semiarid regions. Journal of hydrology 496, 9–16.

Yoder, C.K., Nowak, R.S., 1999. Hydraulic lift among native plant species in the Mojave Desert. Plant and Soil 215, 93–102.

Zhang, K., Zhu, G., Ma, N., Chen, H., Shang, S., 2022. Improvement of evapotranspiration simulation in a physically based ecohydrological model for the groundwater–soil–plant–atmosphere continuum. Journal of Hydrology 613, 128440.

Zhu, G., Zhang, K., Chen, H., Wang, Y., Su, Y., Zhang, Y., Ma, J., 2019. Development and evaluation of a simple hydrologically based model for terrestrial evapotranspiration simulations. Journal of hydrology 577, 123928.

Zhu, J., Young, M., Healey, J., Jasoni, R., Osterberg, J., 2011. Interference of river level changes on riparian zone evapotranspiration estimates from diurnal groundwater level fluctuations. Journal of Hydrology 403, 381–389.